Hypermethylation is associated with increased age in almond (*Prunus dulcis* [Mill.] D.A. Webb) accessions

Katherine M. D'Amico-Willman[1], Chad E. Niederhuth[2], Elizabeth S. Anderson[3], Thomas M. Gradziel[4], Jonathan Fresnedo Ramírez[1,3*]

[1]Translational Plant Sciences Graduate Program, The Ohio State University, Columbus, OH 43210
[2]Department of Plant Biology, Michigan State University, East Lansing, MI 48824
[3]Department of Horticulture and Crop Science, Ohio Agricultural Research and Development Center, The Ohio State University, Wooster, OH 44691
[4]Department of Plant Sciences, University of California, Davis, CA 95616
*For correspondence (fresnedoramirez.1@osu.edu)

Summary

- The focus of this study is to profile changes in DNA methylation occurring with increased age in almond breeding germplasm in an effort to identify possible biomarkers of age that can be used to assess the potential individuals have to develop aging-related disorders in this productive species.

- To profile DNA methylation in almond germplasm, 70 methylomes were generated from almond individuals representing three age cohorts (11, 7, and 2-years old) using an enzymatic methyl-seq approach followed by analysis to call differentially methylated regions (DMRs) within these cohorts.

- Weighted chromosome-level methylation analysis reveals hypermethylation in 11-year-old almond breeding selections when compared to 2-year-old selections in the CG and CHH contexts. A total of 17 consensus DMRs were identified in all age-contrasts, and one of these DMRs contains the sequence for miR156, a microRNA with known involvement in regulating the juvenile-to-adult transition.

- Almond shows a pattern of hypermethylation with increased age, and this increase in methylation may be involved in regulating the vegetative transition in almond. The identified DMRs could function as putative biomarkers of age in almond following validation in additional age groups.

Keywords: DNA methylation, enzymatic methyl-seq, juvenility, miRNA

Total Word Count:

Word Count by Section: Introduction - 677; Materials and Methods - 1902; Results - 1563; Discussion – 2347

Number of Figures: 2

Number of Tables: 3

Number of Supporting Information: 6 Figures; 10 Tables; 2 Files

Introduction

The study of aging has centered primarily around mammalian systems with a focus on humans (Kirkwood, 2005; Ferrucci *et al.*, 2020); however, the aging process has also been shown to impact plants with emphasis placed on long-lived perennials (Munné-Bosch, 2007; Thomas, 2013; Brutovská *et al.*, 2013; Woo *et al.*, 2018). These impacts can include things like diminished growth, reduced flower and fruit production, and the development of aging-related disorders (Kester & Jones, 1970; Van Dijk, 2009). In perennial plants and in other organisms such as humans, causal mechanisms underlying the development of age-related phenotypes include genetic alterations such as somatic mutations or differential epigenetic marks (Jaligot *et al.*, 2000; Dubrovina & Kiselev, 2016; Ogneva *et al.*, 2016; Xiao *et al.*, 2019; Wang *et al.*, 2020). In fact, DNA methylation in particular has been proposed as a biomarker of aging in many systems, serving as a biological "clock" that can be used to track aging and predict aging outcomes (Runov *et al.*, 2015; Jylhävä *et al.*, 2017; Xiao *et al.*, 2019).

Studying epigenetic alterations like differential DNA methylation associated with advanced age in perennial plant systems can (1) provide a means to track aging in these systems and (2) lead to an increased understanding of the development of age-related disorders or degeneration of important physiological processes. This information is valuable to agricultural industries that rely on sustained production of perennial crops, including fruit and nut trees. Almond (*Prunus dulcis* [Mill.] D.A. Webb) is an example of a perennial nut crop that is negatively affected by the aging process through the exhibition of non-infectious bud failure, an aging associated disorder (Kester & Jones, 1970; Micke, 1996; Kester *et al.*, 2004). Additionally, almond trees are primarily produced by clonal propagation for orchard establishment, meaning age, and thus susceptibility to age-related impacts is difficult to determine (Ally *et al.*, 2010; de Witte & Stöcklin, 2010; Salguero-Gomez, 2018). A means to track aging, particularly in crops like almond produced by clonal propagation or shown to exhibit age-related disorders, benefits growers, producers, and consumers by helping to protect the supply chain of these valuable commodities.

Profiling genome-wide DNA methylation is one approach to quantify differential epigenetic marks in an effort to model alterations associated with advanced age. Whole-genome enzymatic methylation sequencing is equivalent to the "gold standard" bisulfite sequencing approach to profile the methylome at the nucleotide level (Feng *et al.*, 2020). Utilizing this

approach provides information on both genome-wide methylation in each context (CG, CHG, and CHH [H = A, T, or C]) and allows for the identification of differentially methylated regions (DMRs), pin-pointing regions of the genome showing dynamic patterns of methylation associated with increased age (Vaisvila *et al.*, 2020; Feng *et al.*, 2020). Identification of specific regions of the genome showing changes in methylation associated with aging provides both the opportunity to develop biomarkers to track aging and information on those genes or genic regions that might contribute to the development of age-related phenotypes (Xiao *et al.*, 2019).

In this study, we utilize almond breeding germplasm grown from seed following pedigreed crosses as part of the almond breeding program at the University of California, Davis. The individuals used in this study are, since grown from seed, of known age and thus particularly useful to generate models to track aging in this species where clonal propagation is standard. The goal of this study was to examine DNA methylation patterns in the genome of a productive perennial crop by performing an exhaustive methylome profiling of ~70 almond individuals from three distinct age-cohorts. The hypothesis is that the almond breeding selection cohorts will exhibit, on average, divergent DNA methylation profiles associated with age. Our overall aim is to identify variability in the almond methylome that could enable model development to track aging in this clonally propagated crop and provide targets (i.e., differentially methylated regions) for further investigation into mechanisms influencing age-related phenotypes such as non-infectious bud failure or the juvenile-to-adult transition. This work additionally serves as a model to explore aging and its impacts in other important perennial crops.

Materials and Methods

Plant Material

Almond leaf samples were collected in May 2019 from the canopy of 30 distinct breeding selections planted in 2008, in 2012, and in 2017, totaling 90 individuals sampled. These selections represent three almond age cohorts aged 11, 7, and 2-years at the time of sampling. Almond breeding germplasm sampled for this study is maintained at the Wolfskill Experimental Orchards (Almond Breeding Program, University of California – Davis, Winters, CA). The pedigree of each sample collected was also documented, including both the female and male parents of each individual. Leaf samples were collected in the field and immediately stored on ice and then at -20 °C until shipping. Samples were shipped on ice to the Ohio Agricultural

Research and Development Center (OARDC; The Ohio State University, Wooster, OH, USA) and immediately stored at -20 °C until sample processing.

DNA Extraction

High-quality DNA was extracted from leaves following a modified version of the protocol outlined in Vilanova *et al.*, 2020. Briefly, samples were ground to a fine powder with a mortar and pestle in liquid nitrogen, and 50 mg of the ground material was added to 1 mL of extraction buffer (2% w/v CTAB; 2% w/v PVP-40; 20 mM EDTA; 100 mM Tris-HCl [pH 8.0]; 1.4 M NaCl), 14 µL beta-mercaptoethanol, and 2 µL RNase (10 mg/mL). The solution was incubated at 65 °C for 30 mins and on ice for 5 mins followed by a phase separation with 700 µL chloroform:isoamyl alcohol (24:1). The aqueous phase (~800 µL) was recovered, and 480 µL binding buffer (2.5 M NaCl; 20% w/v PEG 8000) was added followed by 720 µL 100% ice-cold ethanol.

A silica matrix buffer was prepared by adding 10 g silicon dioxide to 50 mL ultra-pure water prior to incubation and centrifugation steps. Silica matrix buffer (20 µL) was added to each sample, and samples were gently mixed for 5 mins. Samples were spun for 10 secs and the supernatant was removed. To resuspend the remaining mucilaginous material (but not the pellet), 500 µL cold 70% ethanol was used, and supernatant was removed. Another 500 µL cold 70% ethanol was added to resuspend the silica pellet, the tubes were spun for 5 secs, and the supernatant was removed. The pellet was allowed to dry at room temperature for 5 mins and was resuspended in 100 µL elution buffer (10 mM Trish HCl [pH 8.0]; 1 mM EDTA [pH 8.0]) followed by a 5 min incubation at 65 °C. Samples were centrifuged at 14,000 rpm for 10 mins at room temperature and 90 µL of supernatant was transferred to a new tube. DNA concentration was assessed by fluorometry using a Qubit™ 4 and Qubit™ 1X dsDNA HS Assay Kit (ThermoFisher Scientific, Waltham, MA, USA).

Enzymatic Methyl-Seq Library Preparation and Illumina Sequencing

Whole-genome enzymatic methyl-seq libraries were prepared using the NEBNext® Enzymatic Methyl-seq kit (New England BioLabs® Inc., Ipswich, MA, USA) according to the manufacturer's instructions. Each sample was prepared using 100 ng input DNA in 48 µL TE buffer (1 mM Tris-HCl; 0.1 mM EDTA; pH 8.0) with 1 µL spikes of both the CpG unmethylated Lambda and CpG methylated pUC19 control DNA provided in the kit. The samples were

sonicated using a Covaris® S220 focused-ultrasonicator in microTUBE AFA Fiber Pre-Slit Snap-Cap 6×16 mm tubes (Covaris®, Woburn, MA, USA) with the following program parameters: peak incident power (W) = 140; duty factor = 10%; cycles per burst = 200; treatment time (s) = 80.

Following library preparation, library concentration and quality were assessed by fluorometry using a Qubit™ 4 and Qubit™ 1X dsDNA HS Assay Kit (ThermoFisher Scientific) and by electrophoresis using a TapeStation (Agilent, Santa Clara, CA, USA). Library concentration was further quantified by qPCR using the NEBNext® Library Quant Kit for Illumina® (New England BioLabs® Inc.). Libraries were equimolarly pooled in batches of ~15 (five libraries per age cohort) and cleaned using an equal volume of NEBNext® Sample Purification Beads (New England BioLabs® Inc.). The library pools were eluted in 25 µL TE buffer (1 mM Tris-HCl; 0.1 mM EDTA; pH 8.0), and concentration and quality were assessed by fluorometry and electrophoresis as above. Library pools were sequenced on two lanes of the Illumina® HiSeq4000 platform to generate 150-bp paired-end reads.

Processing and Alignment of Enzymatic Methyl-Seq Libraries

Methyl-Seq read quality was initially assessed using FastQC v. 0.11.7 (Andrews, 2010) and reads were trimmed using TrimGalore v. 0.6.6 and Cutadapt v. 2.10 with default parameters (Krueger, 2016). Forward read fastq and reverse read fastq files from the two HiSeq4000 lanes were merged for each library to produce single fastq files for both read one and read two. Reads were aligned to the 'Nonpareil' v. 2.0 almond reference genome, deduplicated, and methylation calls were generated using Bismark v. 0.22.3 (Krueger & Andrews, 2011) with default parameters in paired-end mode. To test conversion efficiency, reads were also aligned to both the Lambda and pUC19 nucleotide sequence fasta files provided by NEB (https://www.neb.com/tools-and-resources/interactive-tools/dna-sequences-and-maps-tool). All analyses were performed using the Ohio Supercomputer Center computing resources (Ohio Supercomputer Center, 1987).

Weighted Genome-wide Methylation Analysis of Age-Cohorts

Weighted genome-wide percent methylation values were calculated for each individual within each cohort by taking the total number of methylated reads at each cytosine and dividing this by the total number of reads (methylated + unmethylated) at each cytosine. Weighted values were calculated for each methylation context. These values were used as input to R v. 4.0.2 (R Core

Team, 2020) to perform beta regression using the package betareg v. 3.1-3 (Cribari-Neto & Zeileis, 2010). Pairwise comparison of least squared means was completed by the functions *emmeans()* and *cld()* from the R packages emmeans v. 1.5.2-1 and multcomp v. 1.4-14 with an alpha = 0.05 and Sidak adjustment (Hothorn *et al.*, 2008). The R package ggplot2 v. 3.3.2 was used to create plots for weighted percent methylation within each methylation-context (Wickham, 2016). Files were then subset by chromosome (chr1 – chr8), and weighted percent methylation values were calculated for all individuals by chromosome using the same formula as above for each methylation context. These values were used as input in R v. 4.0.2 (R Core Team, 2020) to perform beta regression and subsequent pairwise comparison of least squared means as performed above for the genome-wide weighted percent methylation values.

Differential Methylation Analysis of Age-Cohorts

Coverage files for each methylation context produced by Bismark were prepared for input into the R package DSS (Dispersion Shrinkage for Sequencing Data) v. 2.38.0 (Wu *et al.*, 2013; Feng *et al.*, 2014; Park & Wu, 2016). The functions *DMLtest()* and *callDMR()* were used with a significance p.threshold set to 0.0001 to identify differentially methylated regions (DMRs) through pairwise comparisons between the three age cohorts. Comparisons were made relative to the oldest cohort in each DMR test (i.e., 11-year-old cohort relative to 2-year-old cohort).

Classification and annotation of differentially methylated regions

Following identification of DMRs in each age-contrast (11 – 2 year; 11 – 7 year; 7 – 2 year) and methylation-context, DMRs were further characterized based on the directionality of differential methylation. Hypermethylated DMRs are those that show increased methylation in the oldest cohort in each contrast, and hypomethylated DMRs are those that show decreased methylation in the oldest cohort in each contrast. The cumulative binomial probability of identifying an equal or greater number of hypermethylated DMRs in each age-contrast by methylation-context was calculated using the R base package stats command *pbinom()* where x = the number of hypermethylated DMRs in each age-contrast by methylation-context, size = the total number of DMRs identified in each age-contrast/methylation-context, p = 0.5, and lower.tail = FALSE.

To visualize enrichment of DMRs across the eight chromosomes in the 'Nonpareil' genome, circos plots were generated with one track depicting each DMR classified as either hyper- or hypomethylated and two additional tracks depicting DMR enrichment across the genome. To create the circos plots, the R package circlize v. 0.41.2 (Gu *et al.*, 2014) was used

along with the bed files for all hyper- and hypomethylated DMRs in each methylation-context for all age-contrasts. The command *circos.genomicRainfall()* was used to create the first track with dots representing each individual DMR (red – hypermethylated, blue – hypomethylated) and positioned based on the number of DMRs occurring in that location. The command *circos.genomicDensity()* was used to create the two additional tracks representing enrichment of hyper- and hypomethylated DMRs on each chromosome where the taller the peak, the higher the number of DMRs occurring in the specific region (Gu *et al.*, 2014).

Following classification into hyper- and hypomethylated regions, bed files were generated for these DMRs using genomic coordinates. These bed files were used as input along with the 'Nonpareil' genome annotation file into the R v. 4.0.2 (R Core Team, 2020) packages GenomicRanges v. 1.40.0 (Lawrence *et al.*, 2013) and genomation v. 1.20.0 (Akalin *et al.*, 2015) to prepare a GRanges object and annotate DMRs using the command *annotateWithFeatures()*. Initial annotation of DMRs by features includes the percentage of DMRs overlapping one of four features: gene, exon, 5' untranslated region (UTR), and 3' UTR. The DMRs were further annotated, and gene ontology (GO) enrichment was performed using the software HOMER v. 4.11 (Heinz *et al.*, 2010) and the R package topGO v. 2.40.0 (Alexa A, 2020). Initially, all DMRs were annotated by assigning the gene with the closest transcriptional start site to each DMR using *annotatePeaks.pl -noann* with the 'Nonpareil' genome and genome annotation files. This produced a list of gene identifiers from the genome annotation file that are associated with each DMR. The GO terms assigned to each DMR-associated gene were used as input along with the 'Nonpareil' genomic annotation file to determine enrichment of GO terms in each age-contrast DMR-associated gene set. The DMR-associated genes in each methylation-context were classified based on biological process, molecular function, and cellular component GO term to produce tables depicting the number of DMR-associated genes assigned to each descriptor.

The DMRs were then further classified based on the occurrence of overlapping genomic regions among DMRs when comparing age-contrasts. The bed files generated above were used as input in the bedtools v. 2.29.2 (Quinlan & Hall, 2010) command *intersect -wao* to identify overlaps in DMRs from each of the age-contrasts (i.e., 11-7 contrast compared to 11-2 contrast). Finally, genomic regions were identified that contain significant DMRs in all three age-contrasts using bedtools *intersect*. These overlapping DMRs were annotated using the *annotatePeaks.pl* script as above to find DMR-associated genes as well as GO terms, Pfam identifiers, and Interpro

identifiers associated with each gene. The genomic DMR sequence was extracted from the 'Nonpareil' genome fasta file, and individual DMR fasta files were searched against the miRbase database v. 22.1 (Kozomara *et al.*, 2019) to identify any putative microRNAs (miRNAs) within those regions. Searches were performed by sequence using an e-value cutoff of 10 and the *Prunus persica* (L.) Batsch species filter.

Annotation of unknown protein sequences

Genes coding for proteins with unknown function and associated with the DMRs shared across the three age-contrasts were interrogated using *in silico* approaches to characterize the proteins. Several programs were used to annotate these protein sequences and determine additional information about their putative functions. The program ProtParam was used to characterize protein properties including molecular weight (Gasteiger *et al.*, 2005). To predict subcellular localization, the program YLoc was used (Briesemeister *et al.*, 2010a,b). Finally, the Motif tool on the GenomeNet website (https://www.genome.jp/tools/motif/) was used to search a protein query against several databases to identify putative alignments (Marchler-Bauer *et al.*, 2013; Sigrist *et al.*, 2013; Finn *et al.*, 2014).

Results

Genome-wide methylation analysis in almond accessions representing three age-cohorts

Following DNA isolation, library preparation, and Illumina sequencing, a total of 21 almond breeding selections were used for subsequent analysis in the 2-year-old age cohort, 25 in the 7-year-old age cohort, and 24 in the 11-year-old age cohort. Sequencing results show aligned coverage for almond accessions ranged from 3.85 – 50.41X with an average mapping efficiency of 49.8 % (Data S1). Conversion efficiency was greater than 98% based on alignment to the Lambda reference sequence file (Data S1).

Analysis of weighted genome-wide percent methylation within all methylation-contexts (CG, CHG, and CHH) revealed a significant increase in weighted methylation in the 11-year-old age cohort compared to the 2-year-old in the CG (p-value = 0.0105) and CHH (p-value = 0.0399) contexts, respectively (Fig. 1a, c). There was also a significant increase in CG methylation in the 11-year-old age cohort compared to the 7-year-old age cohort (p-value = 0.0115; Fig. 1a). There was not a significant difference in weighted genome-wide methylation in the CHG context when comparing age cohorts (Fig. 1b).

To further analyze weighted methylation in these samples, methylation data for each individual was processed per chromosome, and weighted methylation was analyzed at the chromosome level for each methylation-context. (Figure S1a-c). Pairwise comparisons of DNA methylation within each chromosome revealed significant differences in cytosine methylation on distinct chromosomes for each methylation-context (Table S1a-c). In the CG context, both the 2 – 11 year and the 7 – 11-year age-contrasts were significant on chromosomes 1, 3, 5, 7, and 8 (Table S1). In the CHG context, both the 2 – 11 year and the 7 – 11-year age-contrasts were significant on chromosome 5, the 7 – 11-year age-contrast was significant on chromosome 7, and the 2 – 11-year age-contrast was significant on chromosome 8 (Table S1). Finally, in the CHH context, the 2 – 11-year age-contrast was significant on chromosomes 5, 7, and 8 (Table S1). Overall, significant differences in chromosome-level DNA methylation between age cohorts tend to occur on chromosomes 5, 7, and 8.

Identification and classification of differentially methylated regions (DMRs) between age cohorts

DMRs were identified based on comparisons between the age cohorts in each methylation context. Most DMRs identified are in the CG context, followed by CHH and CHG, respectively (Table 1). These DMRs were further classified as hyper- and hypomethylated based on the amount of methylation in the older cohort compared to the younger. Hypermethylated DMRs have a higher amount of methylation in the older cohort, while hypomethylated DMRs have a higher amount of methylation in the younger cohort for each comparison. In the CG context, 96%, 94%, and 64% of the identified DMRs were hypermethylated in the 11 – 2 year, 11 – 7 year, and 7 – 2-year age-contrasts, respectively (Table 1). In the CHG context, 68%, 52%, and 64% of DMRs were hypermethylated in the 11 – 2 year, 11 – 7 year, and 7 – 2-year age-contrasts, respectively (Table 1). Finally, in the CHH context, 82%, 38%, and 82% of DMRs were hypermethylated in the 11 – 2 year, 11 – 7 year, and 7 – 2-year age-contrasts, respectively (Table 1). The cumulative binomial probability of the occurrence of hypermethylated DMRs was less than 1×10^{-6} for all age-contrasts except 11 – 7 year in the CHG and CHH contexts, suggesting there are more hypermethylated DMRs than would be expected given an equal probability of hyper- and hypomethylated DMRs in the genome. Identified DMRs ranged in length from 51-4824 base pairs (Fig S2a-l). The average length of a gene in the 'Nonpareil' genome is 2,912 bp, so most of the identified DMRs are much shorter than the average gene.

The distribution of CG-context DMRs showed a similar pattern across all chromosomes, where the 11 – 2-year age-contrast has the highest number of DMRs per chromosome, followed by the 11 – 7 year and 7 – 2-year age-contrasts (Fig. S3a). In the CHG and CHH contexts, the distribution of DMRs showed greater variability, with the 11 – 7-year age-contrast typically showing the lowest number of DMRs across all chromosomes, while the 11 – 2 and 11 – 7-year age-contrasts oscillate in number of DMRs occurring on each chromosome across the genome (Fig. S3b,c).

Classification of DMRs as hyper- or hypomethylated in the age cohort comparisons

Using the classifications of hyper- and hypomethylated, DMRs were plotted across the eight chromosomes of the 'Nonpareil' genome revealing unique distributions based on both methylation-context and age-contrast, as well as indicating DMR enrichment in specific chromosomes (Fig. 2). In the CG context, DMR enrichment occurs in the 11 – 2-year age-contrast, with predominantly hypermethylated DMRs, though enrichment of hypomethylated DMRs appears on chromosome 5 (Fig. 2a). The CHG context represents the lowest overall enrichment of DMRs compared to the other methylation-contexts, with regions throughout the genome showing slight enrichment of DMRs (Fig. 2b). Finally, DMRs in the CHH context show similar patterns in enrichment for both the 7 – 2 year and 11 – 2-year age-contrasts, with evident DMR enrichment occurring on chromosomes 3 and 8 (Fig. 2c). The 11 – 7-year age-contrast in the CHH methylation-context is the only contrast to have a higher number of hypomethylated DMRs compared to hypermethylated (Table 1; Fig. 2c).

Following classification of DMRs as either hyper- or hypomethylated in each age-contrast, DMRs were compared among age-contrasts to identify overlapping genomic regions. This analysis revealed several overlapping DMRs from distinct age-contrasts. The highest number of overlaps occurred in CG context hypermethylated DMRs, particularly when comparing the 11 – 2 by 11 – 7 and 11 – 2 by 7 – 2 age-contrasts (Table 2). Interestingly, the 11 – 7 by 7 – 2 age-contrast revealed very few overlaps in hypermethylated DMRs, and no overlapping hypomethylated DMRs (Table 2). Finally, a comparison was performed to identify DMRs with overlapping genomic regions among all three age-contrasts, showing the 11 – 2 age-contrast contains DMRs that share a genomic region with the overlapping DMRs in the 11 – 7 by 7 – 2 comparison (Table 2). This final analysis revealed 17 overlapping DMRs among the three age-contrasts, meaning these DMRs share overlapping genomic coordinates (Table S2). These

17 DMRs are the longest (ranging from 106 – 1,504 base pairs) in the 11 – 2 age-contrast, followed by the 11 – 7 (56 – 713 base pairs) and 7 – 2 (52 – 1,037 base pairs) age contrasts (Table S2). Analysis of the average percent methylation of cytosines within the genomic regions identified in the 11 – 7 age-contrasts shows that in the majority of these regions, cytosines become more methylated with increased age across the three age cohorts (Figs S4a-m, S5a-c, S6).

Annotation of hyper- and hypomethylated differentially methylated regions (DMRs)

An annotation was performed classifying all hyper- and hypomethylated DMRs in each methylation-context into four categories (gene, exon, 5' untranslated region [UTR], and 3' UTR) based on their association with features in the 'Nonpareil' genome annotation. CG context DMRs generally tended to have higher associations with genes and exons compared to the other methylation contexts, while CHG DMRs tended to have higher associations with 5' UTRs and CHH DMRs with 3' UTRs compared to the other contexts (Table S3).

Identified DMRs were then annotated using the 'Nonpareil' genome annotation file to determine the closest gene associated with each DMR. Enrichment analysis was performed for both hyper- and hypomethylated DMR-associated genes in all methylation contexts for each age-contrast, revealing a suite of biological process, molecular function, and cellular component gene ontology (GO) terms associated with each contrast (Tables S4-S9). Comparing annotations between age-contrasts identified GO terms unique to each age-contrast in each methylation-context and degree of methylation (i.e., hyper or hypo). For example, a subset of genes associated with hypermethylated DMRs in the CG context from all three age-contrasts were assigned the molecular function GO terms transmembrane transporter activity, protein serine/threonine kinase activity, and DNA-binding transcription factor activity (Table S4b).

Annotation of genes associated with 17 hypermethylated DMRs identified across the three-age cohort age-contrasts

Of the DMRs identified in each age-contrast, 17 hypermethylated DMRs were found to share genomic regions in all three age-contrasts, meaning these regions showed consistent significant increases in methylation in the older age cohort relative to the younger in each age-contrast. The 17 DMRs were annotated using the 'Nonpareil' genome annotation to identify the closest associated gene. In total, eight previously annotated genes including *FAR1-RELATED SEQUENCE 5* (*FRS5*), a receptor-interacting serine/threonine-protein kinase 4 (*Ripk4*), and

dCTP pyrophosphatase 1 (*Dctpp1*) were identified as associated with nine of the DMRs (Table 3). One CG DMR and one CHG DMR are both associated with the gene Tryptophan aminotransferase-related protein 3 (*TAR3*) (Table 3). The remaining eight DMRs are associated with genes of unknown function (Table 3). These eight unknown protein sequences were used as input into three programs to determine properties including predicted motifs, localization, and weight. Two of these unknown proteins contained transposase_24 motifs, and four are predicted to be localized to the nucleus (Table S10).

In addition to identifying genes associated with these 17 shared DMRs, the DMR genomic sequences (Data S2) were searched against the miRBase database using the *Prunus persica* species filter to identify any potential miRNAs within these regions. Results from this analysis showed that two of the 17 DMRs contain miRNA sequence including CGDMR8 and CHGDMR1. The miRNA identified in CGDMR8 is ppe-miR6276 and ppe-miR156 in CHGDMR1.

Discussion

Perennial plant aging and the impacts of this process, particularly on productive fruit and nut crops, is a neglected area of research with potential applications for agricultural production and crop improvement. The ability to track age in clonally propagated crops could aid in the mitigation of age-related disorders like non-infectious bud failure (Kester *et al.*, 2004) and, more broadly, in overcoming the decrease in plant performance resulting from intense production systems that affect orchard/vineyard longevity. Biomarkers of age in these species, however, are lacking. The aim of this study was to test the hypothesis that, on average, almond breeding selection cohorts will exhibit divergent DNA methylation profiles associated with age. The long-terms goals of this work are to develop biomarkers of age in almond, a clonally propagated crop, and to further our understanding of the aging process in perennial species. To address this, whole-genome DNA methylation profiles were generated for ~70 almond individuals from three distinct age cohorts, and comparisons were made between cohorts to identify regions of interest for further study into their involvement in the aging process and utility as biomarkers of age in almond.

DNA hypermethylation in the CG and CHH contexts is associated with increased age in almond

The DNA methylation profiles generated for individuals in the three age cohorts (11, 7, and 2-years old) were compared at the whole-genome and chromosome level, which showed that hypermethylation in the CG and CHH methylation-contexts is associated with increased age in almond. Further, the probability of identifying the number of hypermethylated DMRs observed in this study was very low for most age-contrasts, suggesting there was a disproportionately high number of hypermethylated DMRs identified compared to hypomethylated DMRs. This result supports previous work theorizing an increase in total genomic DNA methylation with increased age in plants (Dubrovina & Kiselev, 2016). Previous studies have also shown that genome-wide hypermethylation can result in a high number of identified hypermethylated DMRs in subsequent analyses, as was reported in several species including Monterey pine (*Pinus radiata* D.Don), peach (*P. persica*), and coast redwood (*Sequoia sempervirens* [D.Don] Endl.) (Bitonti *et al.*, 2002; Fraga *et al.*, 2002b; Huang *et al.*, 2012).

DNA methylation has been proposed as a "biological clock" capable of predicting the true, ontogenetic age of an individual due to observed patterns of increased methylation with increased age in a variety of species (Runov *et al.*, 2015). Results in this study suggest that almond fits this pattern of hypermethylation, and thus DNA methylation may serve as a biomarker of age in this species. Whole-genome hypermethylation with increased age represents an opportunity to develop high-throughput screening methods that do not require whole-genome sequencing. These methods could include high-performance liquid chromatography or capillary electrophoresis (Stach *et al.*, 2003; Armstrong *et al.*, 2011).

Epigenetic regulation by DNA methylation, histone modifications, and chromatin remodeling has also been shown to modulate the juvenile-to-adult phase transition in plants, including in gymnosperms like Monterey pine and in angiosperms such as peach (Bitonti *et al.*, 2002; Fraga *et al.*, 2002a; Xu *et al.*, 2018). The juvenile period in almond is approximately 3-4 years, thus differential patterns of methylation observed in this study between the 2-year cohort and the 7- and 11-year cohorts could be associated with the juvenile-to-adult transition as has been documented in other plants (Dubrovina & Kiselev, 2016). Patterns of differential methylation identified in this study and associated with specific regions of the genome further demonstrate the potential involvement of DNA methylation in regulating this transition in almond. Further investigation is needed focusing on the involvement of DNA-methylation in the juvenile-to-adult transition in almond and other perennial species, including those with available

transgenic germplasm exhibiting reduced juvenility, such as apple (Flachowsky *et al.*, 2011; Kumar *et al.*, 2020).

Differentially methylated regions (DMRs) in the CG and CHG contexts are enriched on specific chromosomes in the almond genome

Following identification of DMRs in the three age-contrasts, these regions were plotted across the almond genome showing enrichment of DMRs on specific chromosomes, particularly in the CG and CHH methylation-contexts. These so called "hotspots" of differential DNA methylation could suggest loci in these regions are prone to epigenetic alterations including methylation. Transposable elements (TEs) tend to be heavily methylated and have been reported to have involvement in developmental processes in almond, such as the juvenile-to-adult transition (Han *et al.*, 2018; Corso-Díaz *et al.*, 2020; Wyler *et al.*, 2020), suggesting the "hotspots" identified in almond in this study could contain TE sequences. This type of pattern has been documented in other species such as rice, were a study on salt tolerance identified DMRs that tended to cluster on specific chromosomes and were typically associated with TEs on these chromosomes (Ferreira *et al.*, 2019).

In this study, hypermethylated DMRs were enriched on chromosome 8 in the CG context, and on chromosomes 3 and 8 in the CHH context. As increased levels of methylation tend to occur in regions rich in TEs, it is possible that regions enriched in DMRs contain TEs which become increasingly methylated with age. Interestingly, a study in *Brachypodium distachyon* (L.) P.Beauv. found that DMRs were highly correlated with genetic diversity as classified by presence of single nucleotide polymorphisms (SNPs) throughout the genome (Eichten *et al.*, 2016). This genetic diversity was found to be related to the presence of TEs at these sites, potentially contributing to the formation of SNPs as well as leading to differential levels of methylation between the lines tested (Eichten *et al.*, 2016). Given the heterozygosity and diversity in almond germplasm, it may be relevant to compare regions enriched in DMRs from the age-contrasts to SNP data in almond to test for a correlation between increased methylation and genetic diversity, particularly for traits associated with growth and development and length of juvenility.

To identify genetic components involved in the juvenile-to-adult transition in *Prunus*, a study utilizing two almond × peach interspecific populations found a single QTL on chromosome 6 associated with juvenility period, defined as the number of years to first fruit

(Donoso *et al.*, 2016). However, this QTL only explained ~13% of the variability in time to first fruit in these populations, suggesting there may be additional regions influencing this trait (Donoso *et al.*, 2016), as has been observed in other species such as citrus (Raga *et al.*, 2012). Additional work is necessary to explore the genetic variability associated with juvenility in almond to see if chromosomes enriched in DMRs based on age are associated with variation in these traits among almond populations. Further, the TE landscape of regions enriched in DMRs could be characterized to determine if there is an abundance of TEs at these locations, potentially explaining the high number of DMRs observed in these regions. A recent study in almond characterized the TE landscape in the 'Texas' cultivar and compared the distribution of TEs in the genome to that of peach (Alioto *et al.*, 2020). This study revealed not only an increased involvement of TEs in trait diversity in almond compared to peach, but also showed enrichment of TEs on almond chromosomes 3 and 8 (Alioto *et al.*, 2020).

DMRs as potential biomarkers of age in almond

The DMRs identified in this study represent those regions in the genome that showed either an increase or a decrease in cytosine methylation with increased age in almond. The results herein suggest that DMRs tend to be hypermethylated in the age-contrasts, meaning there is an increase in methylation in these regions with increased age in each age-contrast. This pattern fits with the weighted genome-wide methylation patterns showing significant increases in methylation in the CG and CHH contexts between the 2- and 11-year-old age cohorts. Unique, hypermethylated DMRs were identified in each age-contrast, providing information on DNA methylation dynamics associated with age. Regions that show increased methylation in each age contrast are of particular interest due to their potential suitability as biomarkers of age, since these regions show incremental increases in methylation from 2-to-7 years and again from 7-to-11 years old.

Within the DMRs identified in each of the age-contrasts, 17 hypermethylated DMRs were identified with overlapping genomic regions in all three contrasts. Once these regions are validated via DNA methylation profiling in additional almond cohorts of known age, a predictive model could be developed considering cytosine methylation level. This model could be applied to clonal germplasm to predict ontogenetic age, providing a basis to screen germplasm for susceptibility to undesirable, age-related phenotypes. These tools may have implications for germplasm management in breeding, production (orchard), propagation (nursery), and conservation (repository) settings.

The genetic features associated with these specific DMRs could also have involvement in developmental processes, including the juvenile-to-adult transition. To annotate these DMRs, genes were identified with transcriptional start sites close to or overlapping the DMR. Of the 17 DMRs, nine were found to be associated with eight annotated genes. These genes include *FRS5*, a *FAR1-related* protein in the *FAR1* gene family which is involved in light perception and was demonstrated to have involvement in plant development and regulation of aging processes in Arabidopsis (Lin & Wang, 2004; Ma & Li, 2018; Xie *et al.*, 2020). The gene *TAR3* was found to be associated with two of the 17 identified DMRs, one in the CG context and one in the CHG context. This gene is part of a gene family known as *TRYPTOPHAN AMINOTRANSFERASE (TAR)*, whose members are a component of one of the major auxin biosynthetic pathways (Hofmann, 2011). The *TAR* genes are involved in the first step of the pathway, in which tryptophan is converted to indole-3-pyruvic acid, which is subsequently converted to auxin (Brumos *et al.*, 2014). Auxin is a well-known regulator of plant development and senescence processes (Ljung, 2013; Khan *et al.*, 2014; Mueller-Roeber & Balazadeh, 2014). While tryptophan-independent pathways for auxin biosynthesis are present in plants, *TAR* genes are involved in the primary biosynthetic pathway, and disruption of *TAR3* expression could impede auxin production (Hofmann, 2011). These genes and the others identified represent interesting targets for future study on their potential involvement in aging processes in almond, including in the vegetative transition. Additionally, eight proteins of unknown function were identified as associated with the overlapping DMRs. Characterization of these proteins could reveal novel genes with potential functions in plant development and aging in almond.

In addition to identifying nearby genes associated with these DMRs, microRNAs (miRNAs) were also surveyed in these regions. Interestingly, two of the DMRs were found to contain miRNA sequences, including one with the sequence for ppe-miR156, a well-characterized miRNA known to be a major regulator of development and phase transition in plants (Wu *et al.*, 2009). Previous studies have shown that miR156 regulates vegetative phase transition in plants by targeting *SQUAMOSA-PROMOTER BINDING PROTEIN-LIKE (SPL)* genes, inhibiting their expression during juvenility (Wu *et al.*, 2009; Jia *et al.*, 2017). As plants age, miR156 expression is repressed, allowing activation of target genes and inducing the transition to adult (Wu *et al.*, 2009). In fact, studies in both Arabidopsis and maize show that mutants overexpressing miR156 experience prolonged juvenility (Wu & Poethig, 2006; Chuck *et*

al., 2007). A recent study in Arabidopsis showed that light perception via *FAR1*-family genes may also interact with miR156 in regulating plant development (Xie *et al.*, 2020).

Previous work has shown 11 putative members of the miR156 family in peach, suggesting that the miRNA identified in this study could be one of several in this family in almond (Luo *et al.*, 2013); work has shown that the function of miR156 in the aging pathway is conserved in *Prunus* species (Bastías *et al.*, 2016). It has also been proposed that miR156 is regulated by epigenetic modifications (Xu *et al.*, 2018), including DNA methylation, however more work is needed to disentangle epigenetic regulation of miR156 expression as well as to characterize and identify targets of miR156 in almond. Additionally, expression of miR156 has been altered through transgenic approaches in other crops to delay flowering, leading to increased plant biomass or abiotic stress tolerance (Zheng *et al.*, 2016; Kang *et al.*, 2020). Manipulation of miR156 in *Prunus* could lead to potential applications for crop improvement, including decreased juvenility, which could greatly decrease breeding cycles for these crops. Results in this study identified a hypermethylated DMR overlapping miR156 and associated with increased age, suggesting one mode of regulation for this miRNA could be cytosine methylation. Induced DNA methylation using gene-editing techniques could provide a potential avenue for manipulation of miR156 in almond or other *Prunus* species, not only for crop improvement applications, but to also further our understanding of this miRNA in plant development and aging in these crops. Since almond is recalcitrant to tissue culture methods, the application of gene-editing techniques in this species would first require optimization of methods allowing propagation of modified material.

The second miRNA sequence identified was ppe-miR6276, which was first identified as a novel miRNA in Japanese apricot (*P. mume* Sieb. et Zucc) and found to have homology with a miRNA sequence in peach (Gao *et al.*, 2012). This miRNA is currently uncharacterized and could provide an interesting target for further investigation in almond and other *Prunus* species to determine its potential role in the plant aging process.

The study of aging in perennial plants is limited despite the potential applications for agriculture and plant production, particularly for fruit and nut crops. Results from this work show that DNA hypermethylation is associated with age in almond and identifies specific genomic regions that could serve as putative biomarkers of age for this species. Biomarkers of age are valuable for clonally propagated crops, whose ontogenetic age can be difficult to determine, to

screen and select germplasm with low potential for developing age-related disorders. Further, the DMRs identified in this study can be used to guide future studies aimed at increasing our understanding of plant aging and vegetative phase transition in perennials. Perennial plants, including almond, are known for having long juvenile periods which can inhibit breeding and improvement efforts. Epigenetic regulators of phase transition such as DNA methylation could provide another tool for developing perennial crops with shorter juvenile periods, dramatically shortening breeding cycles for these species.

Acknowledgements

We would like to acknowledge Matthew Willman for his assistance with the statistical analysis and preparation of the scripts used to perform the computational analyses for this manuscript. We would also like to acknowledge the Ohio Supercomputer Center for access to computing resources and the Translational Plant Sciences Graduate Program for the fellowship for KMDW. This work was supported by The Ohio State University CFAES-SEEDS program grant # 2019-125, the Almond Board of California Grant HORT35, the U.S. Department of Health and Human Services National Institutes of Health - National Cancer Institute - Cancer Center Support Grant (CCSG) P30CA016058, the USDA National Institute of Food and Agriculture AFRI-EWD Predoctoral Fellowship 2019-67011-29558.

Author Contribution

KMDW and JFR conceptualized and designed the study. KMDW and TMG performed the tissue sampling. KMDW and ESA performed all the laboratory portions of the project. KMDW performed all analyses with the assistance of JFR and CEN. KMDW prepared the manuscript with the assistance of JFR and CEN. All authors contributed to editing the manuscript prior to submission. All the authors approved the submission and revised version of this manuscript.

Data Availability

The 'Nonpareil' almond reference genome v. 2.0 fasta file and gff file and descriptions of the data can be found at https://www.rosaceae.org/publication_datasets. All sequencing data for this project has been deposited to the NCBI Sequence Read Archive under Bioproject PRJNAXXXXX including biosamples: X, Y, and Z. All code used to perform analyses reported in the manuscript can be found at (link to GitHub).

References

Akalin A, Franke V, Vlahoviček K, Mason CE, Schübeler D. **2015**. Genomation: a toolkit to summarize, annotate and visualize genomic intervals. *Bioinformatics* **31**: 1127–1129.

Alexa A RJ. **2020**. *topGO: Enrichment Analysis for Gene Ontology*.

Alioto T, Alexiou KG, Bardil A, Barteri F, Castanera R, Cruz F, Dhingra A, Duval H, Martí ÁF i, Frias L, *et al.* 2020. Transposons played a major role in the diversification between the closely related almond and peach genomes: results from the almond genome sequence. *The Plant Journal* **101**: 455–472.

Ally D, Ritland K, Otto SP. **2010**. Aging in a long-lived clonal tree. *PLOS Biology* **8**: e1000454.

Andrews S. **2010**. *FastQC: A quality control tool for high throughput sequence data*.

Armstrong KM, Bermingham EN, Bassett SA, Treloar BP, Roy NC, Barnett MPG. **2011**. Global DNA methylation measurement by HPLC using low amounts of DNA. *Biotechnology Journal* **6**: 113–117.

Bastías A, Almada R, Rojas P, Donoso JM, Hinrichsen P, Sagredo B. **2016**. Aging gene pathway of microRNAs 156/157 and 172 is altered in juvenile and adult plants from in vitro propagated *Prunus* sp. *Ciencia e investigación agraria* **43**: 429–441.

Bitonti MB, Cozza R, Chiappetta A, Giannino D, Castiglione MR, Dewitte W, Mariotti D, Van Onckelen H, Innocenti AM. **2002**. Distinct nuclear organization, DNA methylation pattern and cytokinin distribution mark juvenile, juvenile□like and adult vegetative apical meristems in peach (*Prunus persica* (L.) Batsch). *Journal of Experimental Botany* **53**: 1047–1054.

Briesemeister S, Rahnenführer J, Kohlbacher O. **2010a**. YLoc—an interpretable web server for predicting subcellular localization. *Nucleic Acids Research* **38**: W497–W502.

Briesemeister S, Rahnenführer J, Kohlbacher O. **2010b**. Going from where to why—interpretable prediction of protein subcellular localization. *Bioinformatics* **26**: 1232–1238.

Brumos J, Alonso JM, Stepanova AN. **2014**. Genetic aspects of auxin biosynthesis and its regulation. *Physiologia Plantarum* **151**: 3–12.

Brutovská E, Sámelová A, Dušička J, Mičieta K. **2013**. Ageing of trees: Application of general ageing theories. *Ageing Research Reviews* **12**: 855–866.

Chuck G, Cigan AM, Saeteurn K, Hake S. **2007**. The heterochronic maize mutant Corngrass1 results from overexpression of a tandem microRNA. *Nature Genetics* **39**: 544–549.

Corso-Díaz X, Gentry J, Rebernick R, Jaeger C, Brooks MJ, van Asten F, Kooragayala K, Gieser L, Nellissery J, Covian R, *et al.* 2020. Genome-wide profiling identifies DNA methylation signatures of aging in rod photoreceptors associated with alterations in energy metabolism. *Cell reports* **31**: 107525.

Cribari-Neto F, Zeileis A. **2010**. Beta regression in R. *Journal of Statistical Software* **34**: 1–24.

Donoso JM, Picañol R, Serra O, Howad W, Alegre S, Arús P, Eduardo I. **2016**. Exploring almond genetic variability useful for peach improvement: mapping major genes and QTLs in two interspecific almond × peach populations. *Molecular Breeding* **36**: 16.

Dubrovina AS, Kiselev KV. **2016**. Age-associated alterations in the somatic mutation and DNA methylation levels in plants (A Weber, Ed.). *Plant Biology* **18**: 185–196.

Eichten SR, Stuart T, Srivastava A, Lister R, Borevitz JO. **2016**. DNA methylation profiles of diverse *Brachypodium distachyon* align with underlying genetic diversity. *Genome Research* **26**: 1520–1531.

Feng H, Conneely KN, Wu H. **2014**. A Bayesian hierarchical model to detect differentially methylated loci from single nucleotide resolution sequencing data. *Nucleic Acids Research* **42**: e69.

Feng S, Zhong Z, Wang M, Jacobsen SE. **2020**. Efficient and accurate determination of genome-wide DNA methylation patterns in *Arabidopsis thaliana* with enzymatic methyl sequencing. *Epigenetics & Chromatin* **13**: 42.

Ferreira LJ, Donoghue MTA, Barros P, Saibo NJ, Santos AP, Oliveira MM. **2019**. Uncovering differentially methylated regions (DMRs) in a salt-tolerant rice variety under stress: One step towards new regulatory regions for enhanced salt tolerance. *Epigenomes* **3**: 4.

Ferrucci L, Gonzalez□Freire M, Fabbri E, Simonsick E, Tanaka T, Moore Z, Salimi S, Sierra F, Cabo R de. **2020**. Measuring biological aging in humans: A quest. *Aging Cell* **19**: e13080.

Finn RD, Bateman A, Clements J, Coggill P, Eberhardt RY, Eddy SR, Heger A, Hetherington K, Holm L, Mistry J, *et al.* 2014. Pfam: the protein families database. *Nucleic Acids Research* **42**: D222-230.

Flachowsky H, Roux P-ML, Peil A, Patocchi A, Richter K, Hanke M-V. **2011**. Application of a high-speed breeding technology to apple (*Malus* × *domestica*) based on transgenic early flowering plants and marker-assisted selection. *New Phytologist* **192**: 364–377.

Fraga M, Cañal M, Rodríguez R. **2002a**. Phase-change related epigenetic and physiological changes in *Pinus radiata* D. Don. *Planta* **215**: 672–678.

Fraga MF, Rodríguez R, Cañal MJ. **2002b**. Genomic DNA methylation–demethylation during aging and reinvigoration of *Pinus radiata*. *Tree Physiology* **22**: 813–816.

Gao Z, Shi T, Luo X, Zhang Z, Zhuang W, Wang L. **2012**. High-throughput sequencing of small RNAs and analysis of differentially expressed microRNAs associated with pistil development in Japanese apricot. *BMC Genomics* **13**: 371.

Gasteiger E, Hoogland C, Gattiker A, Duvaud S, Wilkins MR, Appel RD, Bairoch A. **2005**. Protein identification and analysis tools on the ExPASy server. In: Walker JM, ed. Springer Protocols handbooks. The proteomics protocols handbook. Totowa, NJ: Humana Press, 571–607.

Gu Z, Gu L, Eils R, Schlesner M, Brors B. **2014**. Circlize implements and enhances circular visualization in R. *Bioinformatics* **30**: 2811–2812.

Han Z, Crisp PA, Stelpflug S, Kaeppler SM, Li Q, Springer NM. **2018**. Heritable epigenomic changes to the maize methylome resulting from tissue culture. *Genetics* **209**: 983–995.

Heinz S, Benner C, Spann N, Bertolino E, Lin YC, Laslo P, Cheng JX, Murre C, Singh H, Glass CK. **2010**. Simple combinations of lineage-determining transcription factors prime cis-regulatory elements required for macrophage and B cell identities. *Molecular Cell* **38**: 576–589.

Hofmann NR. **2011**. YUC and TAA1/TAR proteins function in the same pathway for auxin biosynthesis. *The Plant Cell* **23**: 3869.

Hothorn T, Bretz F, Westfall P. **2008**. Simultaneous inference in general parametric models. *Biometrical Journal* **50**: 346–363.

Huang L-C, Hsiao L-J, Pu S-Y, Kuo C-I, Huang B-L, Tseng T-C, Huang H-J, Chen Y-T. **2012**. DNA methylation and genome rearrangement characteristics of phase change in cultured shoots of *Sequoia sempervirens*. *Physiologia Plantarum* **145**: 360–368.

Jaligot E, Rival A, Beulé T, Dussert S, Verdeil J-L. **2000**. Somaclonal variation in oil palm (*Elaeis guineensis* Jacq.): the DNA methylation hypothesis. *Plant Cell Reports* **19**: 684–690.

Jia XL, Chen YK, Xu XZ, Shen F, Zheng QB, Du Z, Wang Y, Wu T, Xu XF, Han ZH, *et al.* **2017**. miR156 switches on vegetative phase change under the regulation of redox signals in apple seedlings. *Scientific Reports* **7**: 14223.

Jylhävä J, Pedersen NL, Hägg S. **2017**. Biological age predictors. *EBioMedicine* **21**: 29–36.

Kang T, Yu C-Y, Liu Y, Song W-M, Bao Y, Guo X-T, Li B, Zhang H-X. **2020**. Subtly manipulated expression of ZmmiR156 in tobacco improves drought and salt tolerance without changing the architecture of transgenic plants. *Frontiers in Plant Science* **10**.

Kester DE, Jones RW. **1970**. Non-infectious bud-failure from breeding programs of almond (*Prunus amygdalas* Batsch). *Journal of the American Society of Horticultural Science* **95**: 492–96.

Kester DE, Shackel KA, Micke WC, Viveros M, Gradziel TM. **2004**. Noninfectious bud failure in 'Carmel' almond: I. Pattern of development in vegetative progeny trees. *Journal of the American Society for Horticultural Science* **129**: 244–249.

Khan M, Rozhon W, Poppenberger B. **2014**. The role of hormones in the aging of plants - A mini-review. *Gerontology* **60**: 49–55.

Kirkwood TBL. **2005**. Understanding the odd science of aging. *Cell* **120**: 437–447.

Kozomara A, Birgaoanu M, Griffiths-Jones S. **2019**. miRBase: from microRNA sequences to function. *Nucleic Acids Research* **47**: D155–D162.

Krueger F. **2016**. *Taking appropriate QC measures or RBBS-type or other Seq-applications with TrimGalore!*

Krueger F, Andrews SR. **2011**. Bismark: a flexible aligner and methylation caller for Bisulfite-Seq applications. *Bioinformatics* **27**: 1571–1572.

Kumar S, Hilario E, Deng CH, Molloy C. **2020**. Turbocharging introgression breeding of perennial fruit crops: a case study on apple. *Horticulture Research* **7**: 1–7.

Lawrence M, Huber W, Pagès H, Aboyoun P, Carlson M, Gentleman R, Morgan MT, Carey VJ. **2013**. Software for computing and annotating genomic ranges. *PLOS Computational Biology* **9**: e1003118.

Lin R, Wang H. **2004**. Arabidopsis *FHY3/FAR1* gene family and distinct roles of its members in light control of Arabidopsis development. *Plant Physiology* **136**: 4010–4022.

Ljung K. **2013**. Auxin metabolism and homeostasis during plant development. *Development* **140**: 943–950.

Luo X, Gao Z, Shi T, Cheng Z, Zhang Z, Ni Z. **2013**. Identification of miRNAs and their target genes in peach (*Prunus persica* L.) using high-throughput sequencing and degradome analysis. *PLOS ONE* **8**: e79090.

Ma L, Li G. **2018**. FAR1-RELATED SEQUENCE (FRS) and FRS-RELATED FACTOR (FRF) family proteins in *Arabidopsis* growth and development. *Frontiers in Plant Science* **9**.

Marchler-Bauer A, Zheng C, Chitsaz F, Derbyshire MK, Geer LY, Geer RC, Gonzales NR, Gwadz M, Hurwitz DI, Lanczycki CJ, *et al.* 2013. CDD: conserved domains and protein three-dimensional structure. *Nucleic Acids Research* **41**: D348-352.

Micke WC. **1996**. *Almond production manual*. UCANR Publications.

Mueller-Roeber B, Balazadeh S. **2014**. Auxin and its role in plant senescence. *Journal of Plant Growth Regulation* **33**: 21–33.

Munné-Bosch S. **2007**. Aging in perennials. *Critical Reviews in Plant Sciences* **26**: 123–138.

Ogneva ZV, Dubrovina AS, Kiselev KV. **2016**. Age-associated alterations in DNA methylation and expression of methyltransferase and demethylase genes in *Arabidopsis thaliana*. *Biologia Plantarum* **60**: 628–634.

Ohio Supercomputer Center. 1987. Ohio Supercomputer Center. Columbus OH: Ohio Supercomputer Center. http://osc.edu/ark:/19495/f5s1ph73.

Park Y, Wu H. **2016**. Differential methylation analysis for BS-seq data under general experimental design. *Bioinformatics* **32**: 1446–1453.

Quinlan AR, Hall IM. **2010**. BEDTools: a flexible suite of utilities for comparing genomic features. *Bioinformatics* **26**: 841–842.

R Core Team. 2020. A Language and Environment for Statistical Computing. R Foundation for Statistical Computing, Vienna, Austria https://www.R-project.org

Raga V, Bernet GP, Carbonell EA, Asins MJ. **2012**. Segregation and linkage analyses in two complex populations derived from the citrus rootstock Cleopatra mandarin. Inheritance of seed reproductive traits. *Tree Genetics & Genomes* **8**: 1061–1071.

Runov AL, Vonsky MS, Mikhelson VM. **2015**. DNA methylation level and telomere length as a basis for modeling of the biological aging clock. *Cell and Tissue Biology* **9**: 261–264.

Salguero-Gomez R. **2018**. Implications of clonality for ageing research. *Evolutionary Ecology* **32**: 9–28.

Sigrist CJA, de Castro E, Cerutti L, Cuche BA, Hulo N, Bridge A, Bougueleret L, Xenarios I. **2013**. New and continuing developments at PROSITE. *Nucleic Acids Research* **41**: D344-347.

Stach D, Schmitz OJ, Stilgenbauer S, Benner A, Döhner H, Wiessler M, Lyko F. **2003**. Capillary electrophoretic analysis of genomic DNA methylation levels. *Nucleic Acids Research* **31**: E2.

Thomas H. **2013**. Senescence, ageing and death of the whole plant. *The New Phytologist* **197**: 696–711.

Vaisvila R, Ponnaluri VKC, Sun Z, Langhorst BW, Saleh L, Guan S, Dai N, Campbell MA, Sexton BS, Marks K, *et al.* 2020. EM-seq: Detection of DNA methylation at single base resolution from picograms of DNA. *bioRxiv*: 2019.12.20.884692.

Van Dijk H. **2009**. Ageing effects in an iteroparous plant species with a variable life span. *Annals of Botany* **104**: 115–124.

Vilanova S, Alonso D, Gramazio P, Plazas M, García-Fortea E, Ferrante P, Schmidt M, Díez MJ, Usadel B, Giuliano G, *et al.* 2020. SILEX: a fast and inexpensive high-quality DNA extraction method suitable for multiple sequencing platforms and recalcitrant plant species. *Plant Methods* **16**: 110.

Wang T, Ma J, Hogan AN, Fong S, Licon K, Tsui B, Kreisberg JF, Adams PD, Carvunis A-R, Bannasch DL, *et al.* 2020. Quantitative translation of dog-to-human aging by conserved remodeling of the DNA methylome. *Cell Systems* **11**: 176-185.e6.

Wickham H. **2016**. *ggplot2: Elegant graphics for data analysis*. Springer-Verlag New York.

de Witte LC, Stöcklin J. **2010**. Longevity of clonal plants: why it matters and how to measure it. *Annals of Botany* **106**: 859–870.

Woo HR, Masclaux-Daubresse C, Lim PO. **2018**. Plant senescence: how plants know when and how to die. *Journal of Experimental Botany* **69**: 715–718.

Wu G, Park MY, Conway SR, Wang J-W, Weigel D, Poethig RS. **2009**. The sequential action of miR156 and miR172 regulates developmental timing in *Arabidopsis*. *Cell* **138**: 750–759.

Wu G, Poethig RS. **2006**. Temporal regulation of shoot development in *Arabidopsis thaliana* by miR156 and its target *SPL3*. *Development* **133**: 3539–3547.

Wu H, Wang C, Wu Z. **2013**. A new shrinkage estimator for dispersion improves differential expression detection in RNA-seq data. *Biostatistics* **14**: 232–243.

Wyler M, Stritt C, Walser J-C, Baroux C, Roulin AC. **2020**. Impact of transposable elements on methylation and gene expression across natural accessions of *Brachypodium distachyon*. *Genome Biology and Evolution* **12**: 1994–2001.

Xiao F-H, Wang H-T, Kong Q-P. **2019**. Dynamic DNA methylation during aging: A “prophet” of age-related outcomes. *Frontiers in Genetics* **10**.

Xie Y, Zhou Q, Zhao Y, Li Q, Liu Y, Ma M, Wang B, Shen R, Zheng Z, Wang H. **2020**. *FHY3* and *FAR1* integrate light signals with the miR156-*SPL* module-mediated aging pathway to regulate *Arabidopsis* flowering. *Molecular Plant* **13**: 483–498.

Xu Y, Zhang L, Wu G. **2018**. Epigenetic regulation of juvenile-to-adult transition in plants. *Frontiers in Plant Science* **9**.

Zheng Q, Liu J, Goff BM, Dinkins RD, Zhu H. **2016**. Genetic manipulation of miR156 for improvement of biomass production and forage quality in red clover. *Crop Science* **56**: 1199–1205.

Figures

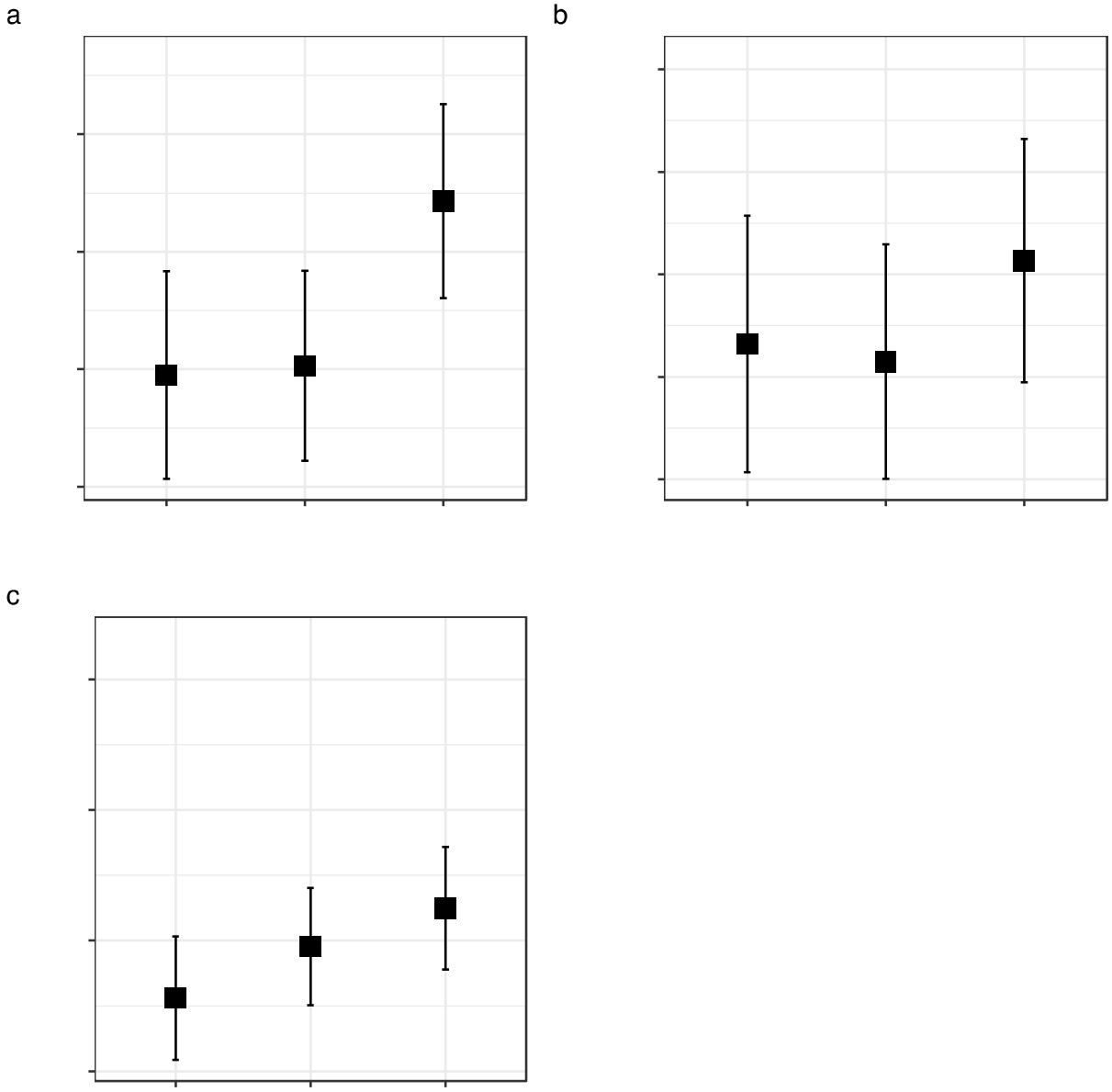

Fig. 1 Proportion of weighted genome-wide methylation in the CG **(a)**, CHG **(b)**, and CHH **(c)** methylation-contexts for each age cohort (2, 7, and 11 years-old). Letter groups represent significant differences based on pairwise comparisons using least squared means (alpha = 0.05).

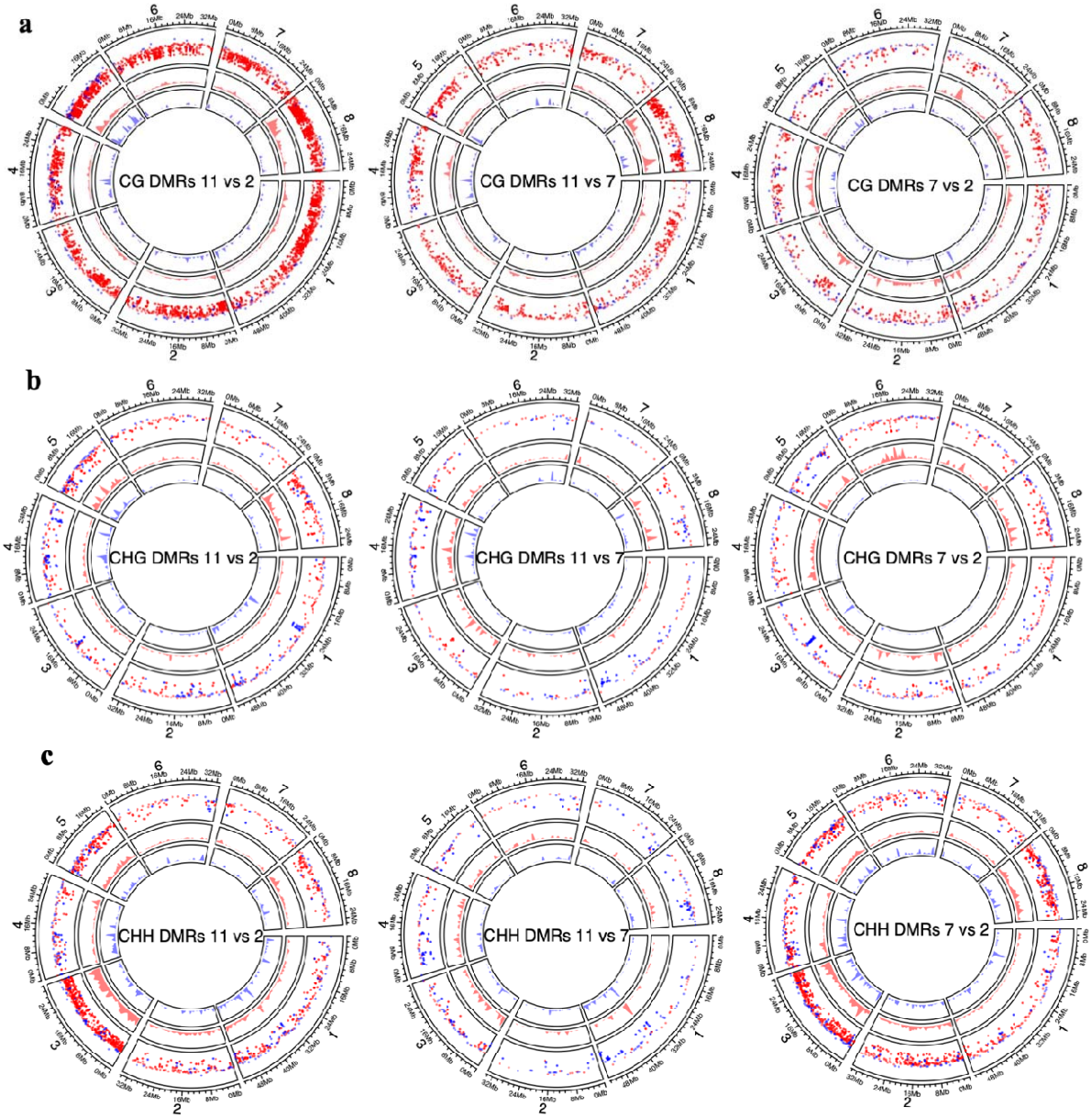

Figure 2a-c. Circos plots depicting individual hyper- (red) and hypo- (blue) methylated differentially methylated regions (DMRs) identified in each contrast and methylation-context. The outer ring of each plot gives approximate location of the individual DMRs on each of the eight 'Nonpareil' chromosomes represented by red and blue dots. The middle ring of each plot represents enrichment of hypermethylated DMRs across each chromosome, and the inner most ring of each plot represents enrichment hypomethylated DMRs across each chromosome. Panel **a** shows the distribution of DMRs in the CG context, panel **b** shows distribution of DMRs in the CHG context, and panel **c** shows distribution of DMRs in the CHH context.

Table 1. Number of identified differentially methylated regions (DMRs) in each methylation-context when comparing the three age cohorts. DMRs were identified with a threshold of $p \leq 0.0001$. DMRs are classified as hypermethylated if the percent methylation in that region is greater in the older age cohort compared to the younger age cohort within each contrast. DMRs are classified as hypomethylated if the percent methylation in that region is lesser in the older age cohort compared to the younger age cohort within each contrast. Hypermethylated DMR values in bold represent those with a cumulative binomial probability $< 1\times10^{-6}$.

Methylation Context	Contrast	Number of DMRs	Hypermethylated DMRs	Hypomethylated DMRs
CG	11-2	6479	**6232**	247
	11-7	2105	**1983**	122
	7-2	1211	**985**	226
CHG	11-2	1129	**763**	366
	11-7	485	252	233
	7-2	813	**524**	289
CHH	11-2	2059	**1690**	369
	11-7	567	216	351
	7-2	2259	**1849**	410

Table 2. Number of occurrences of overlap when comparing differentially methylated regions (DMRs) identified in each contrast to those identified in the other contrasts. The number of overlaps means the number of times a DMR in a particular age-contrast (e.g. 11-2) overlaps the genomic region of a DMR in one of the other age-contrasts (e.g. 11-7). The overall comparison indicates the number of DMRs occurring in overlapping genomic regions in all three contrasts. DMRs are classified as either hyper- or hypomethylated in each methylation context.

Methylation Context	Hyper/Hypo	11-2 ∗ 11-7	11-2 ∗ 7-2	11-7 ∗ 7-2	11-2 ∗ 11-7 ∗ 7-2
CG	Hyper	677	646	13	13
	Hypo	37	58	0	0
CHG	Hyper	75	161	3	3
	Hypo	74	62	0	0
CHH	Hyper	95	607	1	1
	Hypo	78	146	0	0

Table 3. Annotation of genes associated with 17 hypermethylated differentially methylated regions (DMRs) occurring in all three age cohort contrasts. The chromosome (chr) and genomic coordinates (start and end) of each gene are listed along with the gene identification from the 'Nonpareil' genome annotation. Protein identifiers from InterPro and Pfam databases are also included as well as gene ontology (GO) terms associated with the gene.

Methylation Context	Chr	Start	End	GeneID	InterPro	Pfam	GO
CG	chr6	11481648	11484599	*BGLU12*: Beta-glucosidase	IPR001360	PF00232	GO:0004553 GO:0005975
	chr6	5122822	5124703	At3g47570: Probable LRR receptor-like serine/threonine-protein kinase	IPR001245 IPR001611 IPR013210	PF00560 PF07714 PF08263	GO:0004672 GO:0005515 GO:0006468
	chr8	14686870	14697541	Protein of unknown function1			
	chr1	36988003	36989001	*ESD4*: Ubiquitin-like-specific protease	IPR003653	PF02902	GO:0006508 GO:0008234
	chr1	17181984	17183843	Protein of unknown function2	IPR004252	PF03004	
	chr7	7732940	7736793	Protein of unknown function3			
	chr2	12422670	12423066	Protein of unknown function4			
	chr6	3439053	3439763	Protein of unknown function5	IPR009769	PF07059	
	chr8	7299785	7304401	*PS1*: FHA domain-containing protein	IPR000253 IPR002716	PF00498 PF13638	GO:0005515
	chr8	21331964	21333852	*Dctpp1*: dCTP pyrophosphatase 1	IPR025984	PF12643	GO:0009143 GO:0047429
	chr8	7041990	7043388	Protein of unknown function6			
	chr8	5019298	5021435	*TAR3*: Tryptophan aminotransferase-related protein 3	IPR006948	PF04864	GO:0016846
	chr1	1101269	1101943	Protein of unknown function7			
CHG	chr8	7202236	7205963	*FRS5*: Protein FAR1-RELATED	IPR004330	PF03101	GO:0008270

				SEQUENCE 5	IPR007527 IPR018289	PF04434 PF10551 PF13561	
	chr3	20612169	20614252	*Ripk4*: Receptor-interacting serine/threonine-protein kinase 4	IPR020683 IPR026961	PF12796 PF13962	
	chr8	5019298	5021435	*TAR3*: Tryptophan aminotransferase-related protein 3	IPR006948	PF04864	GO:0016846
CHH	chr1	34468253	34469756	Protein of unknown function8			

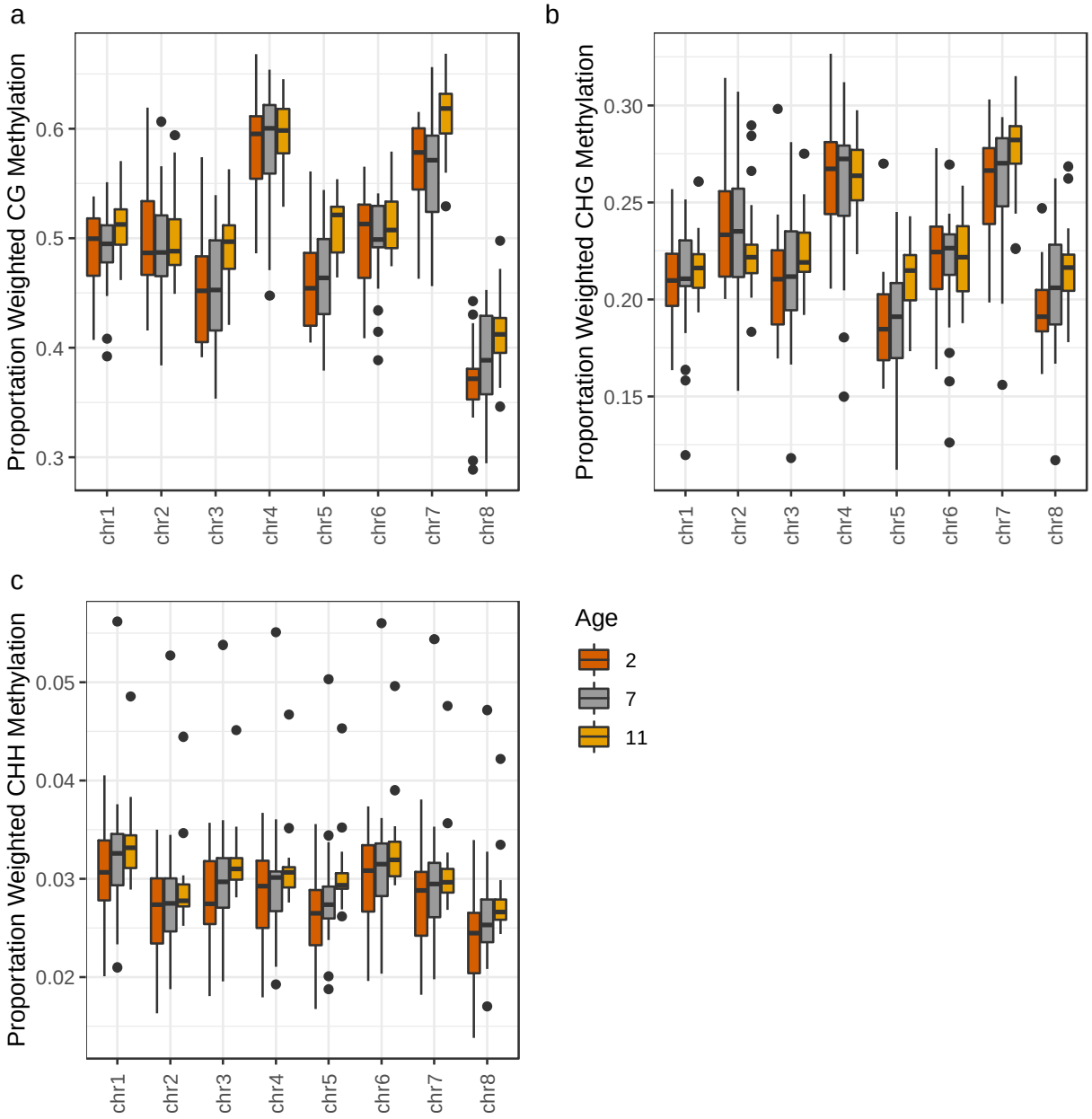

Figure S1. Boxplots depicting the proportion of weighted methylation in each age cohort (2 years old – red; 7 years old – grey; 11 years old – yellow) across the three methylation contexts: **(a)** CG, **(b)** CHG, and **(c)** CHH. The black dots represent outliers.

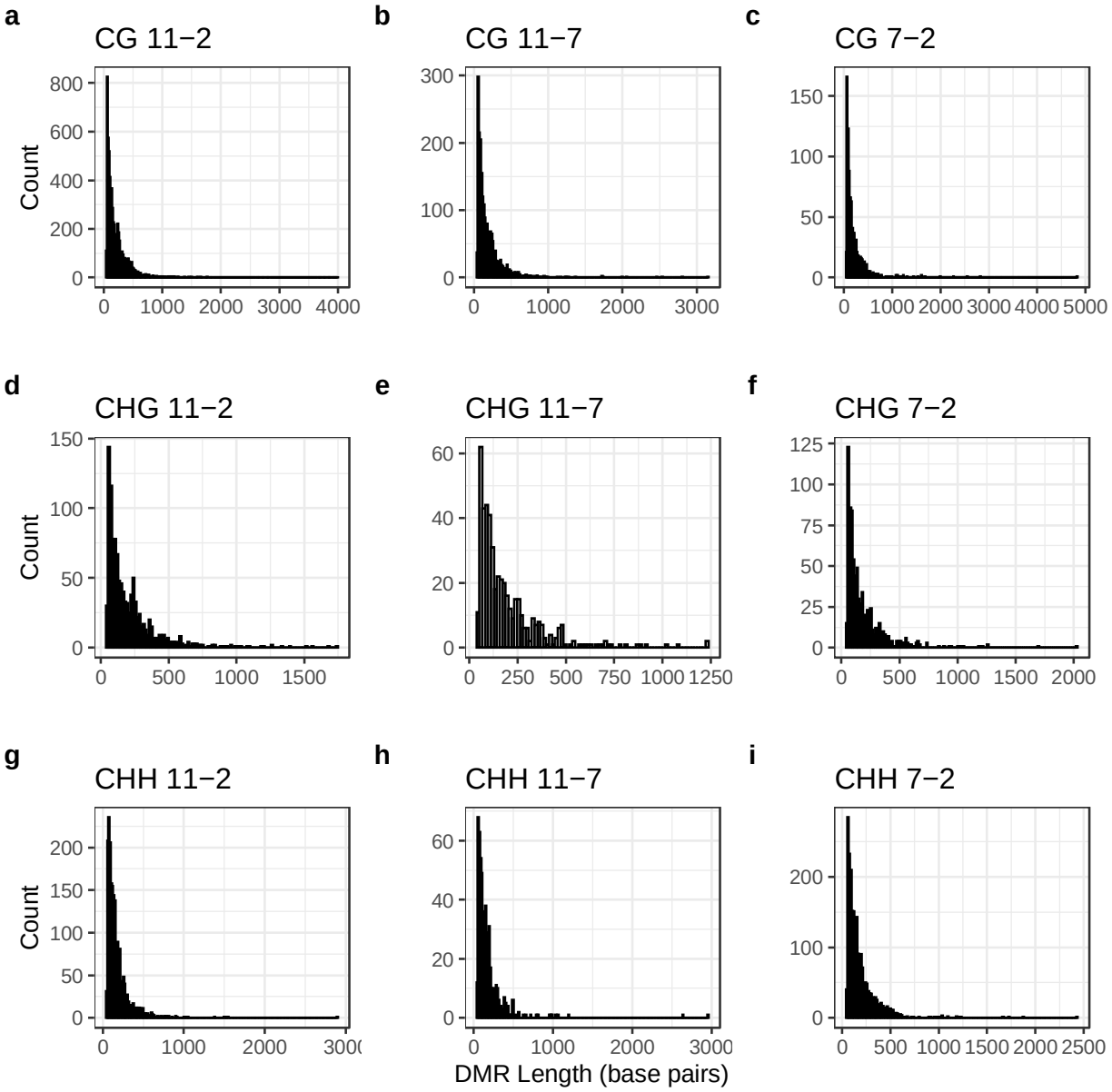

Figure S2a-l. Distribution of lengths in base pairs of differentially methylated regions (DMRs) identified in each age contrast and methylation context. Panels **a-c** show distribution of DMRs identified in the CG context, panels **d-f** show distribution in the CHG context, and panels **g-l** show distribution in the CHH context. The values listed next to the methylation context indicate the age-contrast (11 – 2 year, 11 – 7 year, and 7 – 2 year).

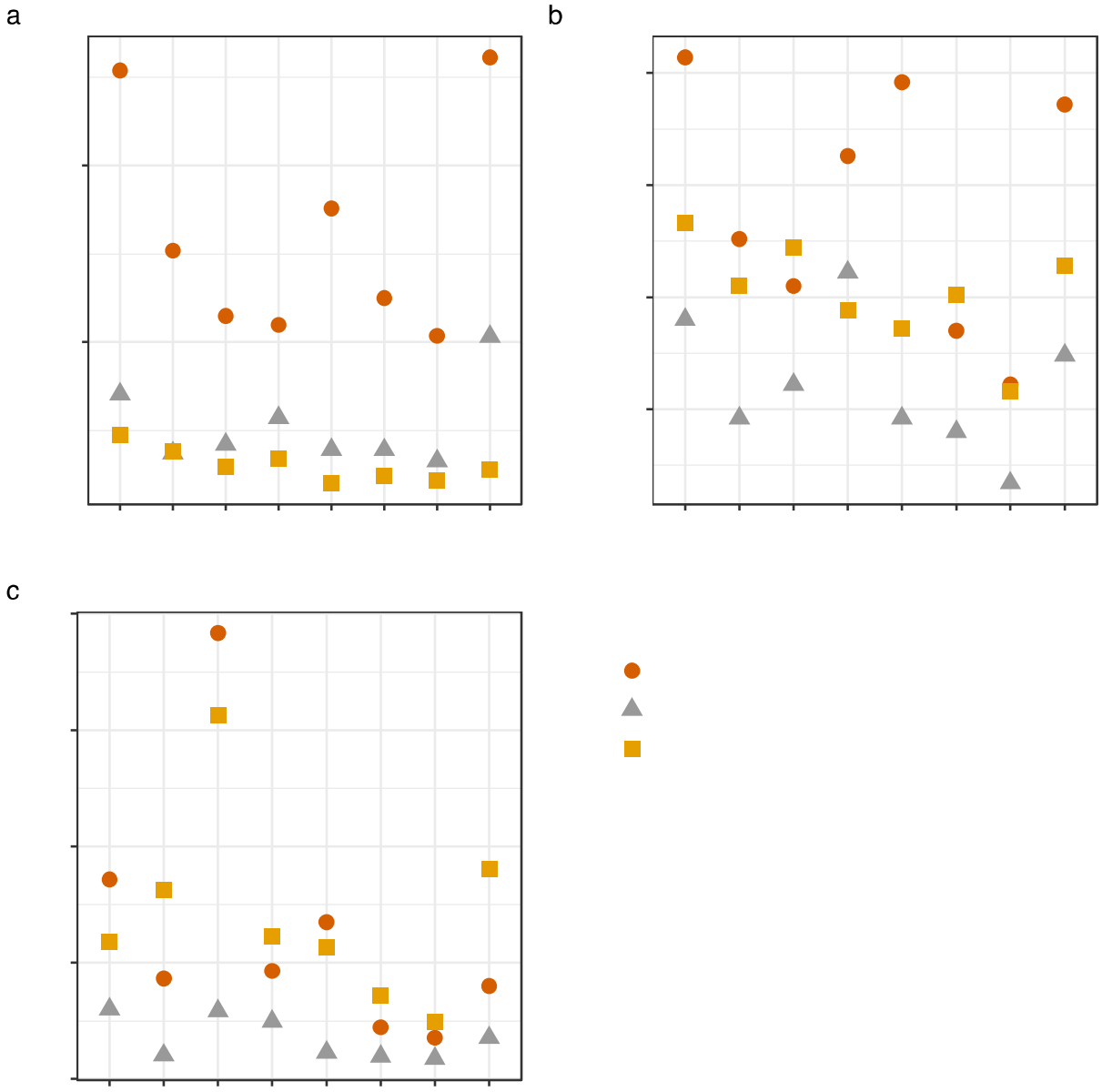

Figure S3a-c. The dot plots represent the number of significant ($p < 0.0001$) differentially methylated regions (DMRs) identified in each of the contrasts (11 – 2 years: red; 11 – 7 years: grey; 7 – 2 years: yellow) in each methylation-context: **(a)** CG, **(b)** CHG, and **(c)** CHH.

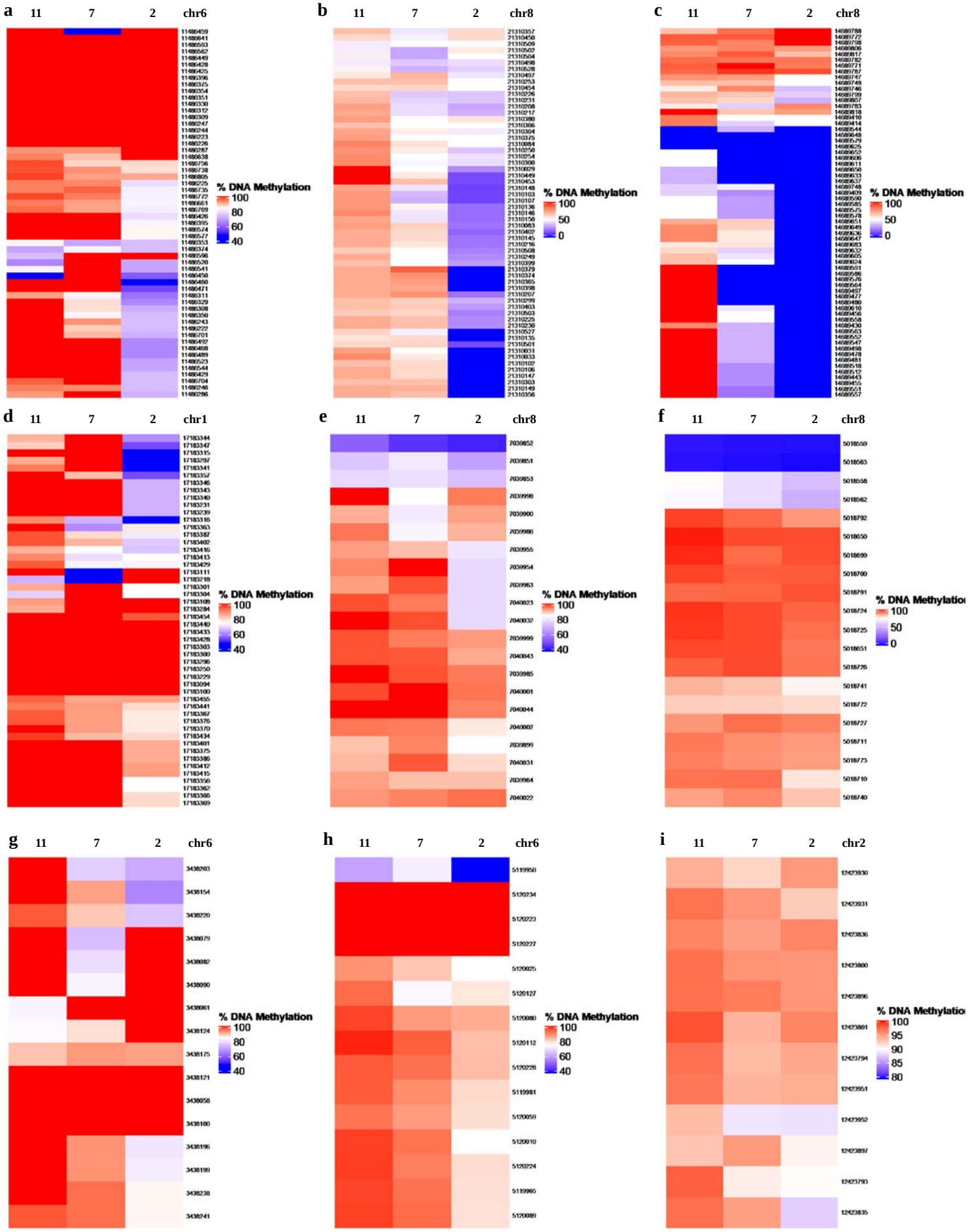
a
11
7
2
chr6
% DNA Methylation
100
80
60
40
b
11
7
2
chr8
% DNA Methylation
100
50
0
c
11
7
2
chr8
% DNA Methylation
100
50
0
d
11
7
2
chr1
% DNA Methylation
100
80
60
40
e
11
7
2
chr8
% DNA Methylation
100
80
60
40
f
11
7
2
chr8
% DNA Methylatio
100
50
0
g
11
7
2
chr6
% DNA Methylation
100
80
60
40
h
11
7
2
chr6
% DNA Methylation
100
80
60
40
i
11
7
2
chr2
% DNA Methylatio
100
95
90
85
80

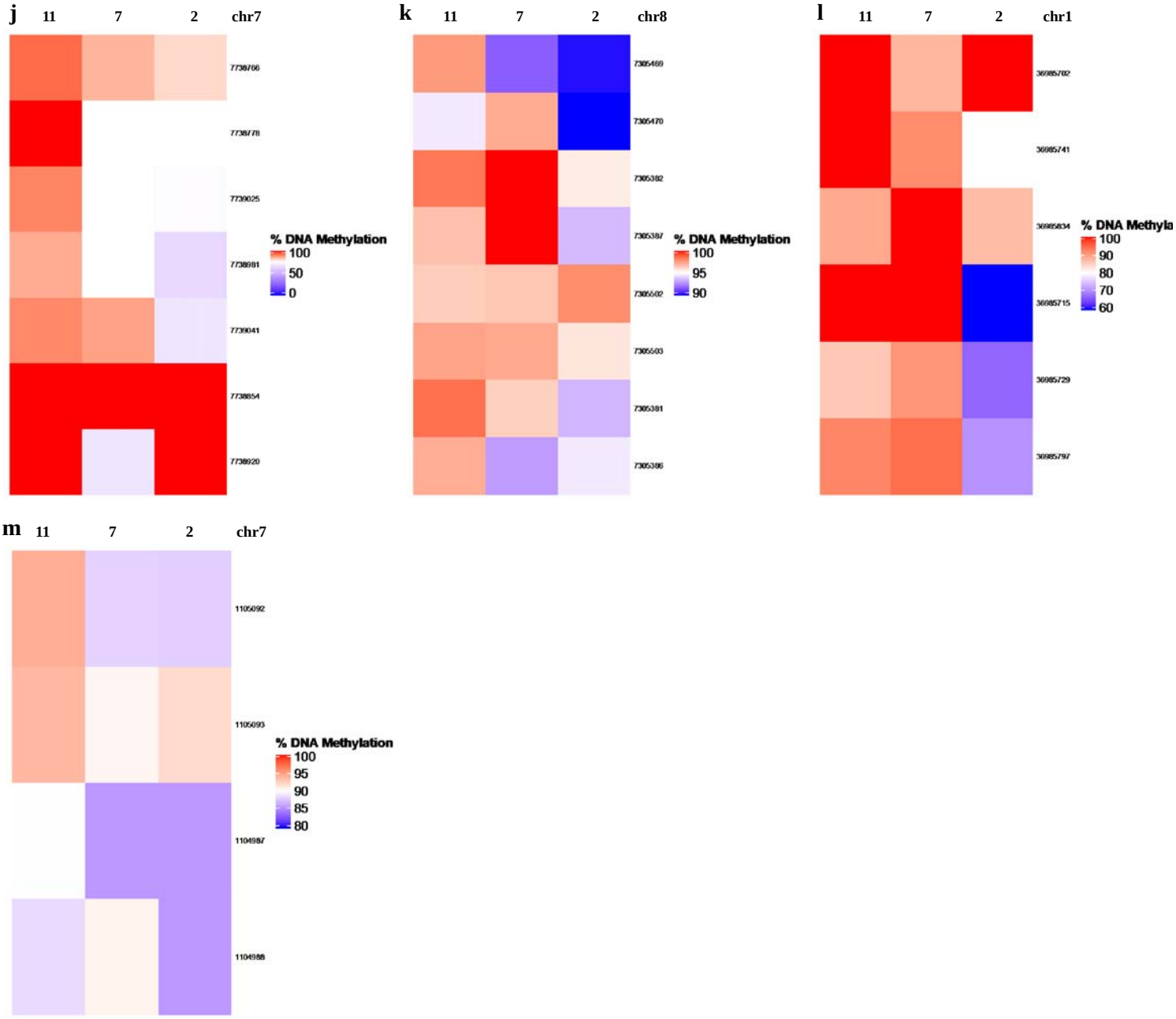

Figure S4a-m. Heatmaps displaying average percent DNA methylation across cytosines in the 11-year, 7-year, and 2-year age cohorts within the genomic range of 13 overlapping differentially methylated regions (DMRs) in the CG context identified in the three age-contrasts. The regions correspond to CGDMR1-13 **(a-m; see Table S2)** and the values to the right of each heatmap represent the genomic position of each cytosine on the respective chromosome.

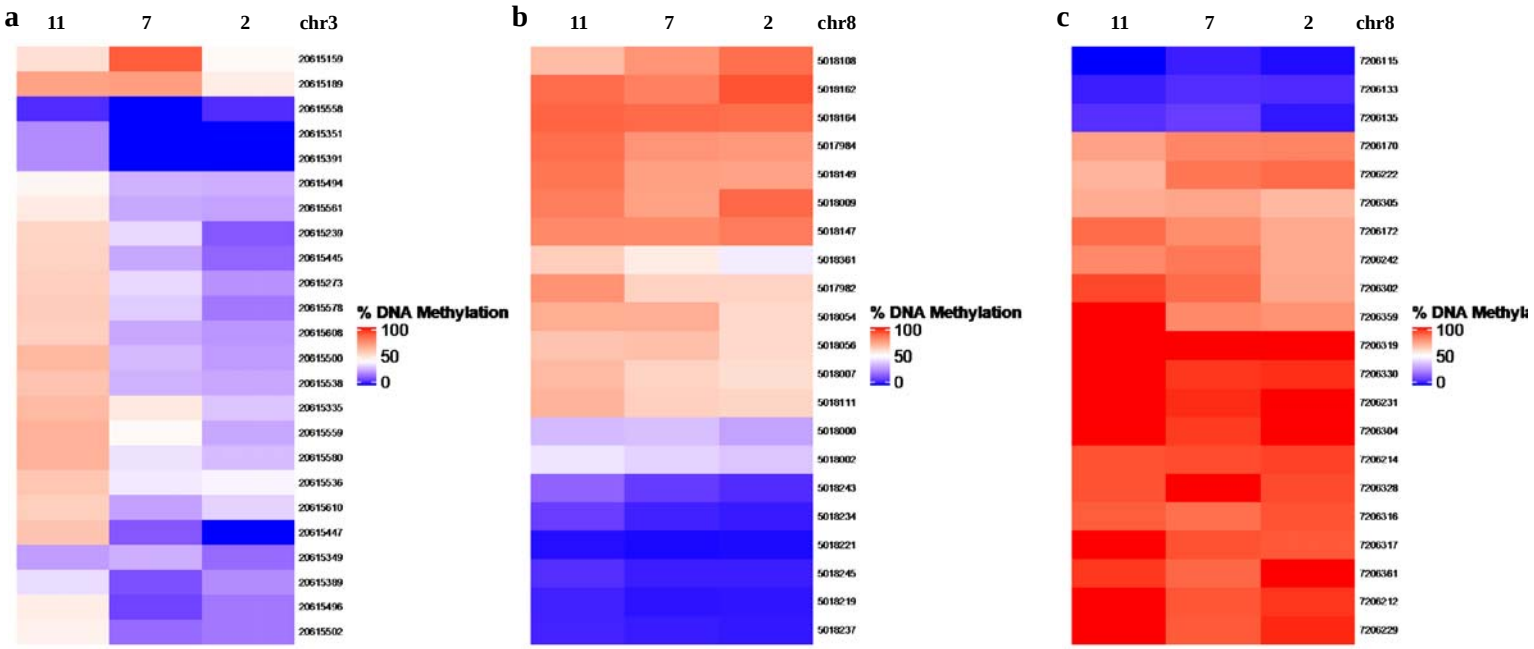

Figure S5a-c. Heatmaps displaying average percent DNA methylation across cytosines in the 11-year, 7-year, and 2-year age cohorts within the genomic range of 3 overlapping differentially methylated regions (DMRs) in the CHG context identified in the three age-contrasts. The regions correspond to CHGDMR1-3 **(a-c; see Table S2)** and the values to the right of each heatmap represent the genomic position of each cytosine on the respective chromosome.

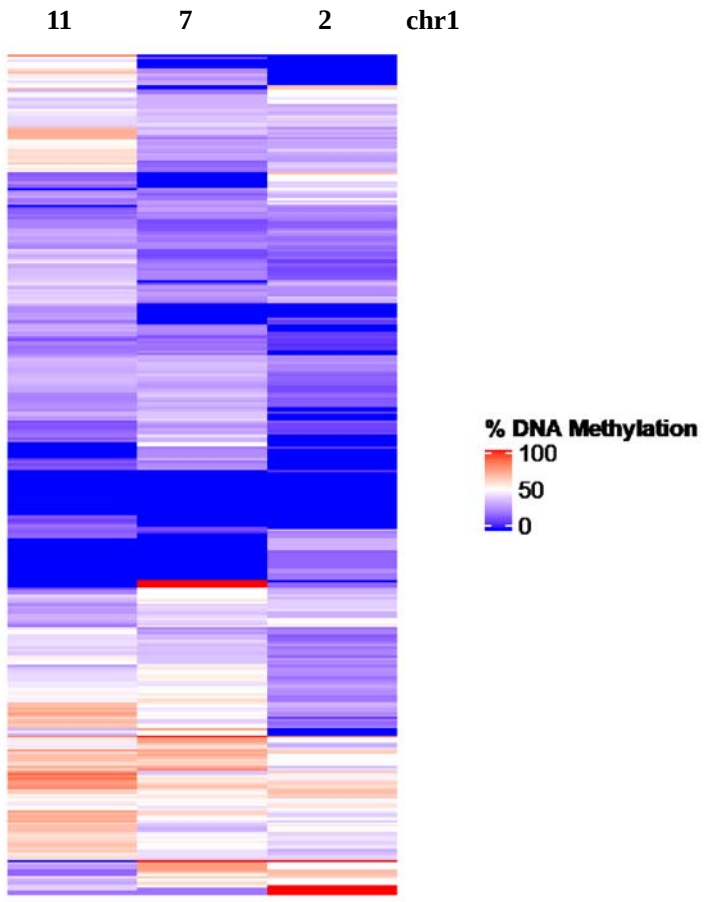

Figure S6. Heatmap displaying average percent DNA methylation across cytosines in the 11-year, 7-year, and 2-year age cohorts within the genomic range of the overlapping differentially methylated region (DMR) in the CHH context identified in the three age-contrasts. The regions correspond to CHHDMR1 **(see Table S2)**.

Table S1. Pairwise comparison of least squared means of weighted percent methylation in the CG, CHG, and CHH contexts for each chromosome in the 'Nonpareil' almond genome. Age cohort contrasts include the 2 – 11, the 7 – 11, and the 2 – 7-year contrasts. Significant contrasts are represented in bold with an alpha = 0.05.

Chromosome	Age-Contrast	CG context p-value	CHG context p-value	CHH context p-value
Chr1	11-2	**0.0235**	0.5329	0.0595
	11-7	**0.0422**	0.4425	0.7068
	7-2	0.9436	0.9949	0.2780
Chr2	11-2	0.9973	0.3587	0.1320
	11-7	0.7356	0.9063	0.6008
	7-2	0.7924	0.5948	0.5698
Chr3	11-2	**0.0020**	0.2137	**0.0138**
	11-7	**0.0046**	0.1647	0.3543
	7-2	0.9267	0.9980	0.2883
Chr4	11-2	0.6659	0.9917	0.0972
	11-7	0.5390	0.8626	0.6030
	7-2	0.9867	0.8071	0.4789
Chr5	11-2	**<.0001**	**0.0056**	**0.0020**
	11-7	**<.0001**	**0.0049**	0.1935
	7-2	0.8706	0.9954	0.1873
Chr6	11-2	0.3472	0.9922	0.0675
	11-7	0.1645	0.7924	0.5824
	7-2	0.9342	0.8679	0.4042
Chr7	11-2	**0.0003**	0.0658	0.0956
	11-7	**0.0002**	**0.0263**	0.7183
	7-2	0.9963	0.9676	0.3716
Chr8	11-2	**0.0004**	**0.0163**	**0.0055**
	11-7	**0.0295**	0.1837	0.4246
	7-2	0.3440	0.5279	0.1329

Table S2. Genomic coordinates and length in base pairs for the 17 overlapping DMRs occurring in each of the three age-contrasts.

		11-2			11-7			7-2		
DMR_ID	**Chr**	**Start**	**End**	**Length (bp)**	**Start**	**End**	**Length (bp)**	**Start**	**End**	**Length (bp)**
CGDMR1	6	11486222	11486807	585	11486637	11486807	170	11486637	11486807	170
CGDMR2	8	21310028	21310528	500	21310028	21310149	121	21310028	21310403	375
CGDMR3	8	14689409	14689818	409	14689430	14689807	377	14689477	14689547	70
CGDMR4	1	17183093	17183455	362	17183249	17183343	94	17183249	17183315	66
CGDMR5	8	7039851	7040044	193	7039954	7040044	90	7039899	7040044	145
CGDMR6	8	5018558	5018792	234	5018650	5018792	142	5018740	5018792	52
CGDMR7	6	3438057	3438262	205	3438026	3438089	63	3438057	3438174	117
CGDMR8	6	5119949	5120234	285	5119949	5120126	177	5119949	5120126	177
CGDMR9	2	12423793	12423952	159	12423835	12423931	96	12423896	12423952	56
CGDMR10	7	7738726	7739046	320	7738980	7739046	66	7738980	7739046	66
CGDMR11	8	7305381	7305503	122	7305386	7305503	117	7305381	7305503	122
CGDMR12	1	36985701	36985875	174	36985796	36985875	79	36985796	36985875	79
CGDMR13	1	1104987	1105093	106	1104987	1105093	106	1104987	1105093	106
CHGDMR1	3	20615159	20615610	451	20615337	20615502	165	20615337	20615391	54
CHGDMR2	8	5017982	5018361	379	5018000	5018056	56	5018000	5018056	56
CHGDMR3	8	7206115	7206361	246	7206170	7206242	72	7206170	7206231	61
CHHDMR1	1	34468252	34469756	1504	34469043	34469756	713	34468083	34469120	1037

Table S3. Annotation of hyper- and hypomethylated differentially methylated regions (DMRs) in each methylation context and for each age-contrast. The 'Nonpareil' genome annotation was used to classify the DMRs into four categories: gene, exon, five prime untranslated region (5' UTR), and three prime untranslated region (3' UTR). The percentages under each classification represent the percentage of DMRs from each methylation-context and contrast in each of the four categories.

Methylation Context	Hyper/Hypo	Contrast	%Gene	%Exon	%5' UTR	%3' UTR
CG	Hyper	11 – 2	28.0	20.6	0.91	0.96
		11 – 7	34.2	25.1	1.51	1.46
		7 – 2	27.8	21.4	0.81	1.32
	Hypo	11 – 2	39.7	31.2	7.29	1.21
		11 – 7	22.1	14.8	0.82	3.28
		7 – 2	29.2	22.1	2.65	0.88
CHG	Hyper	11 – 2	27.7	20.1	2.49	1.70
		11 – 7	24.6	18.3	3.17	1.98
		7 – 2	24.8	17.2	1.91	0.76
	Hypo	11 – 2	23.5	17.8	3.28	1.37
		11 – 7	27.9	18.5	3.00	2.58
		7 – 2	19.4	13.8	2.77	0
CHH	Hyper	11 – 2	18.0	9.41	1.60	2.13
		11 – 7	19.0	12.0	0.46	1.39
		7 – 2	17.9	9.20	1.35	2.16
	Hypo	11 – 2	27.4	14.6	3.25	1.63
		11 – 7	24.5	14.0	3.99	1.99
		7 – 2	24.4	14.2	1.22	1.22

Table S4a-c. Number of CG hypermethylated DMR-associated genes associated with each biological process (**A)**, molecular function **(B)**, and cellular component **(C)** gene ontology (GO) terms for each of the three age-contrasts (i.e., 11 – 2 year, 11 – 7 year, and 7 – 2 year). Values in each column represent the number of DMR-associated genes that are associated with each GO term. Black squares indicate no genes associated with that contrast were assigned the particular GO term.

A. Biological Process GO Term	**11-2**	**11-7**	**7-2**
proteolysis	37	36	8
protein phosphorylation	29	28	7
obsolete oxidation-reduction process	28	22	4
transmembrane transport	18	16	4
regulation of transcription, DNA-templated	9	13	2
carbohydrate metabolic process	10	11	4
steroid biosynthetic process	5		
tRNA aminoacylation for protein translation	3		
signal transduction	1	8	
translation	2	8	
biosynthetic process	1	7	
transcription, DNA-templated	1	7	1
DNA topological change		6	
cation transport	2	4	
endoplasmic reticulum to Golgi vesicle-mediated transport		3	
nitrogen compound metabolic process		3	1
proteolysis involved in cellular protein catabolic process		3	
tRNA processing	3	3	
ATP synthesis coupled proton transport		2	
attachment of GPI anchor to protein		2	
cell redox homeostasis		2	
cell wall modification		2	
defense response		2	
fatty acid biosynthetic process		2	
histone lysine methylation	2		
lipid metabolic process	1	2	
metal ion transport		2	
nucleotide-excision repair	2		
proteasome-mediated ubiquitin-dependent protein catabolic process	2		
recognition of pollen		2	
translational initiation		2	
cell wall macromolecule catabolic process		1	
cellular glucan metabolic process		1	
cellular modified amino acid biosynthetic process	1	1	

cellulose biosynthetic process	1		1
chitin catabolic process		1	
dephosphorylation		1	
DNA replication		1	
DNA-templated transcription, termination	1		
drug transmembrane transport		1	
endoplasmic reticulum organization		1	
fatty acid beta-oxidation	2	1	
glutamine biosynthetic process		1	
intermembrane lipid transfer		1	
intracellular protein transport		1	
intracellular transport		1	
ion transport		1	
malate transport	1		
mitochondrial pyruvate transmembrane transport		1	
mRNA processing		1	
nucleobase-containing compound metabolic process		1	
nucleotide transmembrane transport		1	
nucleotide transport			1
nucleosome assembly		1	
phosphatidylserine biosynthetic process		1	
photosynthesis	1		
photosynthesis, light reaction		1	
photosynthetic electron transport in photosystem II		1	
phytochromobilin biosynthetic process		1	
potassium ion transport		1	
protein folding	2	1	
protein kinase C-activating G protein-coupled receptor signaling pathway	1		
protein neddylation		1	
protein ubiquitination	1	1	
proton transmembrane transport	1		
pseudouridine synthesis			1
pyrimidine nucleotide-sugar transmembrane transport		1	
regulation of translational fidelity	1		
response to auxin			1
response to hormone		1	
RNA modification			1
RNA processing		1	
rRNA processing		1	
sucrose metabolic process		1	1
translation termination			1
terpenoid biosynthetic process	1		
trehalose biosynthetic process	1		
tRNA wobble uridine modification		1	

B. Molecular Function GO Term	11-2	11-7	7-2
ATP binding	41	33	11
cysteine-type peptidase activity	36	32	8
hydrolase activity, acting on ester bonds	26	28	4
protein binding	35	27	10
protein kinase activity	18	26	5
DNA binding	13	20	5
zinc ion binding	20	20	7
ADP binding	3	18	
nucleic acid binding	18	16	3
oxidoreductase activity	3	13	1
transferase activity, transferring hexosyl groups		11	3
catalytic activity	4	9	
DNA-binding transcription factor activity	7	8	1
structural constituent of ribosome	2	8	
DNA topoisomerase activity		6	
transmembrane transporter activity	3	6	1
hydrolase activity, hydrolyzing O-glycosyl compounds	6	5	2
polygalacturonase activity	4	5	2
RNA binding	1	5	1
sequence-specific DNA binding	1	5	
transferase activity, transferring acyl groups other than amino-acyl groups	3	5	1
acetylglucosaminyltransferase activity	1	4	
aminoacyl-tRNA ligase activity	3		
DNA-directed 5'-3' RNA polymerase activity	1	4	1
heme binding	10	4	
iron ion binding	10	4	
lyase activity	4	4	
magnesium ion binding	4	4	
nucleotide binding	3		
oxidoreductase activity, acting on paired donors, with incorporation or reduction of molecular oxygen	9	4	
phosphatidylinositol binding			4
protein dimerization activity	4	4	1
RNA-DNA hybrid ribonuclease activity	10	4	2
solute:proton antiporter activity	1	4	
terpene synthase activity	4	4	
GTP binding	4	3	1
GTPase activity		3	1
hydrolase activity	1	3	
oxidoreductase activity, acting on the CH-OH group of donors, NAD or NADP as acceptor	5	3	
threonine-type endopeptidase activity		3	
3-beta-hydroxy-delta5-steroid dehydrogenase activity	5		

ATPase activity	7	2	1
calcium ion binding	1	2	
copper ion binding	1	2	
damaged DNA binding	2		
electron transfer activity		2	
enzyme inhibitor activity	2	2	
histone-lysine N-methyltransferase activity	2		
metal ion binding		2	
methyltransferase activity	2	2	
nickel cation binding		2	
nutrient reservoir activity	2		1
O-methyltransferase activity	1	2	
obsolete coenzyme binding	2	2	
oxidoreductase activity, acting on NAD(P)H, oxygen as acceptor	1	2	
pectinesterase activity		2	
peroxidase activity	2	2	
protein disulfide oxidoreductase activity		2	
protein serine/threonine kinase activity	11	2	2
proton transmembrane transporter activity		2	
serine-type carboxypeptidase activity		2	
serine-type endopeptidase activity	2	2	
transcription factor binding	2		
transferase activity, transferring acyl groups	2		1
translation initiation factor activity		2	
2-C-methyl-D-erythritol 2,4-cyclodiphosphate synthase activity	1		
3'-5' exonuclease activity		1	
acetyl-CoA carboxylase activity		1	
acyl-CoA oxidase activity	2	1	
antioxidant activity		1	
antiporter activity	1	1	
ATPase-coupled transmembrane transporter activity	5	1	1
ATP:ADP antiporter activity			1
cation transmembrane transporter activity	1		
cellulose synthase (UDP-forming) activity	1		1
channel activity	1	1	
chitin binding		1	
chitinase activity		1	
cobalt ion binding		1	
diacylglycerol kinase activity	1		
DNA-directed DNA polymerase activity		1	
electron transporter, transferring electrons within the cyclic electron transport pathway of photosynthesis activity		1	
endonuclease activity		1	
endopeptidase inhibitor activity	1	1	
FAD binding	1		

glutamate-ammonia ligase activity		1	
glutamate-cysteine ligase activity	1	1	
glycerol-3-phosphate O-acyltransferase activity	1		
GTPase activator activity	1	1	
helicase activity		1	
inorganic diphosphatase activity	1		
intramolecular lyase activity		1	
intramolecular transferase activity, phosphotransferases		1	
ion channel activity		1	
lipid binding		1	
lipid transfer activity		1	
iron-sulfur cluster binding	1		
malate dehydrogenase (decarboxylating) (NAD+) activity		1	
metal ion transmembrane transporter activity		1	
metallopeptidase activity		1	
NAD binding		1	
NEDD8 activating enzyme activity		1	
nucleoside transmembrane transporter activity		1	
oxidoreductase activity, acting on single donors with incorporation of molecular oxygen, incorporation of two atoms of oxygen		1	
oxidoreductase activity, acting on the CH-CH group of donors	2	1	
oxidoreductase activity, acting on the CH-CH group of donors, iron-sulfur protein as acceptor		1	
peptide-methionine (S)-S-oxide reductase activity	4	1	
peptidyl-prolyl cis-trans isomerase activity		1	
phospho-N-acetylmuramoyl-pentapeptide-transferase activity		1	
polysaccharide binding		1	
protein tyrosine/serine/threonine phosphatase activity		1	
pseudouridine synthase activity			1
pyridoxal phosphate binding	1	1	
pyrimidine nucleotide-sugar transmembrane transporter activity		1	
pyrophosphate hydrolysis-driven proton transmembrane transporter activity	1		
racemase activity, acting on amino acids and derivatives			1
strictosidine synthase activity		1	
sucrose synthase activity		1	1
translation release factor activity			1
ubiquitin-like modifier activating enzyme activity		1	
ubiquitin-protein transferase activity	1	1	
unfolded protein binding	2	1	
uridylyltransferase activity		1	
xyloglucan:xyloglucosyl transferase activity		1	

C. Cellular Component GO Term	11-2	11-7	7-2
integral component of membrane	16	18	4
membrane	10	16	4
nucleus	5	9	2
ribosome	2	8	
endoplasmic reticulum	2		
endoplasmic reticulum membrane		4	
proteasome core complex		3	
cytoplasm		2	
GPI-anchor transamidase complex		2	
mitochondrial proton-transporting ATP synthase complex, coupling factor F(o)		2	
nucleolus	2		
nucleosome		2	
acetyl-CoA carboxylase complex		1	
apoplast		1	
cell wall		1	
chromosome		1	
elongator holoenzyme complex		1	
Golgi membrane		1	
Las1 complex		1	
mitochondrial inner membrane		1	
nuclear pore		1	
peroxisome	2	1	
photosystem I	1		
photosystem I reaction center	1		

Table S5a-c. Number of CG hypomethylated DMR-associated genes associated with each biological process (**A)**, molecular function **(B)**, and cellular component **(C)** gene ontology (GO) terms for each of the three age-contrasts (i.e. 11 – 2 year, 11 – 7 year, and 7 – 2 year). Values in each column represent the number of DMR-associated genes that are associated with each GO term. Black squares indicate no genes associated with that contrast were assigned the particular GO term.

A. Biological Process GO Term	**11-2**	**11-7**	7-2
protein phosphorylation	5	1	8
proteolysis	4		7
cell redox homeostasis	3	1	
regulation of transcription, DNA-templated	3	2	7
cellulose biosynthetic process	2		1
obsolete oxidation-reduction process	2	2	12
signal transduction	2		
translational elongation	2		
transmembrane transport	2	1	
tRNA aminoacylation for protein translation	2	1	
ubiquitin-dependent protein catabolic process			2
ATP synthesis coupled proton transport	1		
biosynthetic process	1		1
carbohydrate metabolic process	1	1	4
carboxylic acid metabolic process			1
cell wall modification			1
defense response			1
detection of visible light	1		
dolichol-linked oligosaccharide biosynthetic process	1		1
glutaminyl-tRNA aminoacylation	1		
Golgi vesicle transport	1	1	
histone lysine methylation	1		
intracellular protein transport	1		
photosynthesis			1
protein-chromophore linkage	1		
protein ubiquitination			1
proteolysis involved in cellular protein catabolic process			1
response to oxidative stress			1
transcription, DNA-templated			1
translation	1	2	3
trehalose biosynthetic process	1		1
tRNA aminoacylation	1		
tRNA aminoacylation for protein translation			1

B. Molecular Function GO Term	11-2	11-7	7-2
protein binding	13	3	14
ATP binding	8	4	9
protein kinase activity	5	1	8
cysteine-type peptidase activity	4		7
heme binding	1	2	7
DNA binding	1	2	6
iron ion binding	1	2	6
oxidoreductase activity, acting on paired donors, with incorporation or reduction of molecular oxygen	1	2	6
transferase activity, transferring hexosyl groups	1	1	5
zinc ion binding	5	1	5
catalytic activity	4	3	4
DNA-binding transcription factor activity	1	1	4
hydrolase activity, hydrolyzing O-glycosyl compounds			4
electron transfer activity	3	1	
nucleic acid binding	4	1	3
oxidoreductase activity	1		3
protein disulfide oxidoreductase activity	3		
sequence-specific DNA binding	1		3
structural constituent of ribosome	1	2	3
acetylglucosaminyltransferase activity			2
ADP binding	1	1	2
carbohydrate binding	2	1	
GTP binding		1	2
pyridoxal phosphate binding	1		2
RNA-DNA hybrid ribonuclease activity			2
translation elongation factor activity	2		
transmembrane transporter activity	1		2
actin binding			1
aminoacyl-tRNA ligase activity	2	1	1
ATPase activity	1	1	
ATPase-coupled transmembrane transporter activity	1	1	
calcium ion binding			1
carbon-sulfur lyase activity			1
carbonate dehydratase activity	1		1
carboxy-lyase activity			1
cellulose synthase (UDP-forming) activity	2		1
channel activity			1
copper ion binding			1
DNA-directed 5'-3' RNA polymerase activity			1
double-stranded DNA binding			1
endopeptidase activity			1
enzyme inhibitor activity			1
flavin adenine dinucleotide binding			1

galactose binding	1		
glutamine-tRNA ligase activity	1		
GTPase activity		1	
histone-lysine N-methyltransferase activity	1		
hydrolase activity			1
hydrolase activity, acting on ester bonds			1
kinase activity			1
Lys48-specific deubiquitinase activity		1	
lyase activity	1	2	
magnesium ion binding	1	2	
manganese ion binding			1
metal ion binding			1
metallopeptidase activity			1
methyltransferase activity	1	1	
nucleotide binding	2	1	1
obsolete coenzyme binding			1
oxidoreductase activity, acting on CH-OH group of donors			1
oxidoreductase activity, acting on single donors with incorporation of molecular oxygen, incorporation of two atoms of oxygen	1		1
pectinesterase activity			1
peroxidase activity			1
phospho-N-acetylmuramoyl-pentapeptide-transferase activity			1
phospholipid binding		1	
phosphorelay sensor kinase activity	1		
polygalacturonase activity	1	1	1
protein dimerization activity		1	1
protein-containing complex binding			1
proton-transporting ATP synthase activity, rotational mechanism	1		
RNA binding	1	1	
serine-type endopeptidase activity	1		
terpene synthase activity	1	2	
thiol-dependent ubiquitin-specific protease activity		1	
threonine-type endopeptidase activity			1
transferase activity, transferring acyl groups other than amino-acyl groups	1	2	
translation initiation factor activity	1		
ubiquitin-ubiquitin ligase activity			1
uridylyltransferase activity	1		1

C. Cellular Component GO Term	11-2	11-7	7-2
membrane	6	2	6
integral component of membrane	5	1	3
ribosome	1	2	3
cytoplasm	2		
nucleus	2	1	2
eukaryotic translation initiation factor 3 complex	1		
mitochondrial proton-transporting ATP synthase complex, catalytic sector F(1)	1		
mitochondrion	1		1
photosystem II			1
proteasome core complex			1
proteasome core complex, alpha-subunit complex			1
ubiquitin ligase complex			1

Table S6a-c. Number of CHG hypermethylated DMR-associated genes associated with each biological process (**A)**, molecular function **(B)**, and cellular component **(C)** gene ontology (GO) terms for each of the three age-contrasts (i.e. 11 – 2 year, 11 – 7 year, and 7 – 2 year). Values in each column represent the number of DMR-associated genes that are associated with each GO term. Black squares indicate no genes associated with that contrast were assigned the particular GO term.

A. Biological Process GO Term	**11-2**	**11-7**	**7-2**
proteolysis	16	16	4
obsolete oxidation-reduction process	7	13	2
protein phosphorylation	5	11	5
carbohydrate metabolic process	4	4	
regulation of transcription, DNA-templated	4	4	2
transmembrane transport	5	4	2
positive regulation of stomatal complex development		3	
biosynthetic process	1	2	1
fatty acid biosynthetic process		2	
nitrogen compound metabolic process	2		1
protein ubiquitination		2	
response to auxin	2		
signal transduction	5	2	1
translational termination	2		1
cation transport		1	
cell population proliferation		1	
cell redox homeostasis	1	1	
cell wall modification		1	1
DNA topological change	1		
drug transmembrane transport			1
glycerolipid biosynthetic process	1		
intracellular protein transport		1	
intracellular signal transduction	1	1	
ion transport	1		
lipid metabolic process	1	1	
mistmatch repair	1		
nucleoside metabolic process	1		1
nucleosome assembly		1	
potassium ion transport		1	
recognition of pollen			1
response to oxidative stress		1	2
terpenoid biosynthetic process	1		
transcription, DNA-templated		1	1
translation	2	1	1

vesicle-mediated transport	[redacted]	1	[redacted]

B. Molecular Function GO Term	11-2	11-7	7-2
cysteine-type peptidase activity	14	15	2
protein binding	14	9	7
ATP binding	10	7	8
zinc ion binding	8	3	6
nucleic acid binding	7	4	1
ADP binding	5	5	1
protein kinase activity	5	11	5
hydrolase activity, hydrolyzing O-glycosyl compounds		4	
catalytic activity	3	2	
copper ion binding		3	
DNA binding	3	2	6
RNA-DNA hybrid ribonuclease activity	3	1	
transmembrane transporter activity	3	3	1
actin binding	2		1
endopeptidase inhibitor activity	2	2	
GTP binding	2		
heme binding	2	5	2
hydrolase activity, acting on ester bonds	2	8	2
hydrolase activity, acting on glycosyl bonds		2	
iron ion binding	2	4	
nickel cation binding	2		
oxidoreductase activity, acting on paired donors, with incorporation or reduction of molecular oxygen	2	4	
polygalacturonase activity	2		
protein dimerization activity	2	3	
RNA binding		2	
sequence-specific DNA binding	2	2	
serine-type endopeptidase activity	2	1	
structural constituent of ribosome	2	1	1
translation release factor activity	2		1
ubiquitin-protein transferase activity		2	
2-C-methyl-D-erythritol 2,4-cyclodiphosphate synthase activity	1		
acid phosphatase activity			1
alpha-amylase activity	1		
antioxidant activity		1	
ATP-dependent peptidase activity	1		
ATPase activity			1
calcium ion binding	1	1	
diacylglycerol O-acyltransferase activity	1		
DNA topoisomerase activity	1		
DNA-binding transcription factor activity	1	1	1
DNA-directed 5'-3' RNA polymerase activity			1
double-stranded DNA binding	1		
electron transfer activity	1	1	

endonuclease activity		1	
enzyme inhibitor activity		1	1
flavin adenine dinucleotide binding	1		
growth factor activity		1	
GTPase activator activity	1	1	
hydrolase activity		1	2
ion channel activity	1		
ionotropic glutamate receptor activity	1		
lyase activity		1	
magnesium ion binding		1	
malonyl-CoA decarboxylase activity		1	
metal ion binding		1	2
mismatched DNA binding	1		
NAD binding		1	
nutrient reservoir activity	1		
oxidoreductase activity	1	6	
oxidoreductase activity, acting on CH-OH group of donors	1		
oxidoreductase activity, acting on the aldehyde or oxo group of donors, NAD or NADP as acceptor	1		
oxidoreductase activity, acting on the CH-CH group of donors, NAD or NADP as acceptor		1	
pectinesterase activity		1	1
peptide-methionine (S)-S-oxide reductase activity	1	1	
peroxidase activity		1	2
phosphotransferase activity, alcohol group as acceptor	1		
polysaccharide binding	1		
protein disulfide oxidoreductase activity	1	1	
protein phosphatase regulator activity	1	1	
racemase activity, acting on amino acids and derivatives			1
ribonuclease activity		1	
serine-type carboxypeptidase activity	1		2
solute:proton antiporter activity		1	
strictosidine synthase activity			1
terpene synthase activity		1	
transferase activity, transferring acyl groups		1	1
transferase activity, transferring acyl groups other than amino-acyl groups	1	2	2
transferase activity, transferring hexosyl groups	1		1
ubiquitin-like modifier activating enzyme activity	1		1

C. Cellular Component GO Term	11-2	11-7	7-2
membrane	5	4	1
integral component of membrane	1	3	1
AP-5 adaptor complex		1	
COPI vesicle coat		1	
extracellular region		1	
membrane coat		1	
nucleus	2	1	4
protein phosphatase type 2A complex	1	1	
proton-transporting two-sector ATPase complex, catalytic domain		1	
ribosome	2	1	1
membrane		4	

Table S7a-c. Number of CHG hypomethylated DMR-associated genes associated with each biological process (**A)**, molecular function **(B)**, and cellular component **(C)** gene ontology (GO) terms for each of the three age-contrasts (i.e. 11 – 2 year, 11 – 7 year, and 7 – 2 year). Values in each column represent the number of DMR-associated genes that are associated with each GO term. Black squares indicate no genes associated with that contrast were assigned the particular GO term.

A. Biological Process GO Term	**11-2**	**11-7**	**7-2**
obsolete oxidation-reduction process	5	3	9
protein phosphorylation	5	5	6
proteolysis	5	8	8
regulation of transcription, DNA-templated	4	5	2
carbohydrate metabolic process	2		2
cysteinyl-tRNA aminoacylation	2		
phospholipid biosynthetic process			2
response to auxin	2		1
transmembrane transport	2	1	5
amine metabolic process	1		1
ATP metabolic process	1		
autophagy	1		
base-excision repair		1	
cell redox homeostasis	1		
defense response			1
drug transmembrane transport	1	1	
G protein-coupled receptor signaling pathway	1		
intracellular protein transport		1	
lipid biosynthetic process	1		1
magnesium ion transport	1		
metal ion transport	1	1	
mistmatch repair			1
nucleobase-containing compound metabolic process		1	
nucleosome assembly			1
organic substance metabolic process			1
proton transmembrane transport	1		
purine nucleobase biosynthetic process	1	1	
regulation of cyclin-dependent protein serine/threonine kinase activity			1
response to oxidative stress			1
rRNA processing			1
steroid biosynthetic process		1	
transcription, DNA-templated		1	
translation	1	2	2

translational elongation	1	1	
trehalose biosynthetic process			1
tRNA processing			1
ubiquitin-dependent protein catabolic process			1

B. Molecular Function GO Term	**11-2**	**11-7**	**7-2**
ATP binding	10	5	10
protein binding	9	3	9
zinc ion binding	8	5	8
cysteine-type peptidase activity	5	7	7
DNA binding	5	5	1
protein kinase activity	5	5	6
iron ion binding	4	2	5
heme binding	3	2	5
nucleic acid binding	3	2	5
oxidoreductase activity, acting on paired donors, with incorporation or reduction of molecular oxygen	3	2	4
transferase activity, transferring acyl groups other than amino-acyl groups	3		
3'-5' exonuclease activity		1	
catalytic activity	2	3	2
cysteine-tRNA ligase activity	2		
DNA-binding transcription factor activity	2	2	1
hydrolase activity	2	2	1
hydrolase activity, hydrolyzing O-glycosyl compounds	2		1
Lys48-specific deubiquitinase activity	2		
metal ion binding	2	4	
methyltransferase activity		2	
nucleotide binding	2		
phosphatidylserine decarboxylase activity			2
sequence-specific DNA binding	2	1	1
serine-type endopeptidase activity	2		
thiol-dependent ubiquitin-specific protease activity	2		
acid phosphatase activity	1	2	
ADP binding	1	1	2
aminopeptidase activity			1
ATPase activity			1
calcium ion binding	1	1	
calcium-dependent phospholipid binding	1	1	
carbohydrate binding	1	1	
carbon-sulfur lyase activity			1
chromatin binding			1
copper ion binding	1		1
DNA-3-methyladenine glycosylase activity		1	
DNA-directed 5'-3' RNA polymerase activity		1	
electron transfer activity	1		
endopeptidase inhibitor activity			1
enzyme inhibitor activity			1
flavin adenine dinucleotide binding			1
glycopeptide alpha-N-acetylgalactosaminidase activity	1		

GTPase activity			1
hydrolase activity, acting on ester bonds	1	1	
intramolecular transferase activity, phosphotransferases			1
ionotropic glutamate receptor activity	1	1	
lyase activity	1	2	
magnesium ion binding	1	2	
magnesium ion transmembrane transporter activity	1		
mismatched DNA binding			1
oxidoreductase activity	1	1	2
peroxidase activity			1
phospholipid binding	1	1	
phosphoribosylamine-glycine ligase activity	1	1	
polysaccharide binding		1	
primary amine oxidase activity	1		1
protein dimerization activity	1		2
protein disulfide oxidoreductase activity	1		
protein kinase binding			1
protein serine/threonine kinase activity		1	1
quinone binding	1		1
RNA-DNA hybrid ribonuclease activity	1	1	2
RNA binding		1	
serine-type carboxypeptidase activity		1	
structural constituent of ribosome	1	2	2
terpene synthase activity	1	2	
transferase activity, transferring glycosyl groups			1
transferase activity, transferring hexosyl groups	1	1	
translation elongation factor activity	1	1	
transmembrane transporter activity	1		3
tRNA dihydrouridine synthase activity			1
ubiquitin protein ligase binding			1

C. Cellular Component GO Term	11-2	11-7	7-2
integral component of membrane	4	1	3
cytoplasm	3		
membrane	1	2	3
nucleus	1	1	3
ribosome	1	2	2
anchored component of plasma membrane			1

Table S8a-c. Number of CHH hypermethylated DMR-associated genes associated with each biological process (**A)**, molecular function **(B)**, and cellular component **(C)** gene ontology (GO) terms for each of the three age-contrasts (i.e. 11 – 2 year, 11 – 7 year, and 7 – 2 year). Values in each column represent the number of DMR-associated genes that are associated with each GO term. Black squares indicate no genes associated with that contrast were assigned the particular GO term.

A. Biological Process GO Term	**11-2**	**11-7**	**7-2**
protein phosphorylation	14	7	28
proteolysis	13	6	21
obsolete oxidation-reduction process	8	4	20
regulation of transcription, DNA-templated	7	2	15
translation	1	2	8
transmembrane transport	5	4	8
signal transduction	3	1	6
carbohydrate metabolic process	2	2	4
defense response		1	3
tRNA aminoacylation for protein translation	1		3
cation transport		2	
cell redox homeostasis	1		2
cell wall modification		1	2
DNA topological change			2
exocytosis			2
fatty acid beta-oxidation			2
histone lysine methylation			2
lipid metabolic process		2	2
nitrate assimilation	3		2
positive regulation of Notch signaling pathway	2		
protein ubiquitination			2
pyrimidine nucleotide biosynthetic process	2		
transcription, DNA-templated			2
ATP metabolic process			1
biosynthetic process	1		1
carboxylic acid metabolic process		1	
cell wall biogenesis	1		
cell wall macromolecule catabolic process			1
cellular amino acid metabolic process		1	
cellular glucan metabolic process		1	
cellulose biosynthetic process			1
cellulose microfibril organization	1		1
chitin catabolic process			1
DNA-templated transcription, initiation		1	

drug transmembrane transport			1
endocytosis			1
fatty acid biosynthetic process		1	1
glutathione biosynthetic process		1	
glycolytic process	1		1
glycyl-tRNA aminoacylation			1
guanosine tetraphosphate metabolic process	1		
intermembrane lipid transfer			1
intracellular protein transport	1		1
intracellular signal transduction			1
ion transport	1		1
lipid catabolic process		2	1
malate transport		1	
mannose metabolic process	2		1
mRNA export from nucleus	2		1
nucleobase-containing compound metabolic process			1
nucleosome assembly			1
phosphatidylinositol metabolic process	1		1
phospholipid biosynthetic process		1	
photosynthesis			1
proteasome assembly	2		1
protein kinase C-activating G protein-coupled receptor signaling pathway	1		
protein neddylation			1
protein peptidyl-prolyl isomerization		1	
proteolysis involved in cellular protein catabolic process		1	
proton transmembrane transport			1
regulation of systemic acquired resistance	1		
RNA processing	1		
response to oxidative stress	1		
retrograde vesicle-mediated transport, Golgi to endoplasmic reticulum			1
ribosome biogenesis		1	1
rRNA processing			1
sulfate transport		1	
terpenoid biosynthetic process	1		
transcription by RNA polymerase II			1
transcription initiation from RNA polymerase II promoter	1	1	1
translational elongation			1
tryptophan catabolic process to kynurenine			1
tryptophan metabolic process		1	
ubiquitin-dependent protein catabolic process		1	1
valyl-tRNA aminoacylation			1
vesicle docking involved in exocytosis			1
vesicle-mediated transport	1		1

B. Molecular Function GO Term	11-2	11-7	7-2
protein binding	20	6	42
ATP binding	21	10	37
protein kinase activity	14	7	28
cysteine-type peptidase activity	12	4	20
DNA binding	8	1	19
ADP binding	5	3	16
nucleic acid binding	11	5	15
zinc ion binding	8	2	14
hydrolase activity, acting on ester bonds	5	4	13
protein dimerization activity	5	1	13
structural constituent of ribosome	1	2	8
oxidoreductase activity	7	1	7
DNA-binding transcription factor activity	2	1	6
RNA binding	1		6
acetylglucosaminyltransferase activity	2	1	5
RNA-DNA hybrid ribonuclease activity	4		5
3-hydroxyisobutyryl-CoA hydrolase activity			4
heme binding	2	1	4
iron ion binding	1	1	4
nucleotide binding	1		4
oxidoreductase activity, acting on paired donors, with incorporation or reduction of molecular oxygen	1	1	4
polysaccharide binding	1	2	4
sequence-specific DNA binding	2	1	4
transferase activity, transferring acyl groups	2		4
aminoacyl-tRNA ligase activity	1		3
ATPase activity	5	1	3
calcium ion binding	1		3
catalytic activity	4	3	3
electron transfer activity	1		3
GTPase activity	3		
hydrolase activity			3
oxidoreductase activity, acting on the CH-CH group of donors			3
serine-type endopeptidase activity	1	1	3
transferase activity, transferring hexosyl groups	4	1	3
ubiquitin-like modifier activating enzyme activity	1		3
acyl-CoA oxidase activity			2
DNA topoisomerase activity			2
flavin adenine dinucleotide binding			2
GTP binding	5	1	2
helicase activity			2
histone-lysine N-methyltransferase activity			2
hydrolase activity, hydrolyzing O-glycosyl compounds		1	2
metal ion binding		2	2

methyltransferase activity			2
molybdenum ion binding	3		2
nutrient reservoir activity	2		
oxidoreductase activity, acting on CH-OH group of donors			2
pectinesterase activity		1	2
protein disulfide oxidoreductase activity	1		2
solute:proton antiporter activity		2	
transferase activity, transferring glycosyl groups			2
ubiquitin-protein transferase activity			2
1-deoxy-D-xylulose-5-phosphate synthase activity	1		
3'-5' exonuclease activity			1
alpha-amylase activity	1		
alpha-mannosidase activity	2		1
antioxidant activity			1
arylformamidase activity			1
ATPase-coupled transmembrane transporter activity			1
calcium-dependent phospholipid binding			1
carboxy-lyase activity		1	
cellulose synthase (UDP-forming) activity			1
channel activity		1	1
chitin binding			1
chitinase activity			1
chromatin binding		2	1
copper ion binding	1		1
cysteine-type endopeptidase inhibitor activity			1
diacylglycerol kinase activity	1		
DNA topoisomerase type II (double strand cut, ATP-hydrolyzing) activity			1
DNA-directed 5'-3' RNA polymerase activity			1
endopeptidase activity		1	
enzyme inhibitor activity		2	1
galactoside 2-alpha-L-fucosyltransferase activity	1		
glutathione synthase activity		1	
glycine-tRNA ligase activity			1
glycopeptide alpha-N-acetylgalactosaminidase activity	1		
heat shock protein binding			1
ion channel activity	1		1
lipid transfer activity			1
magnesium ion binding	2		1
mannosyl-glycoprotein endo-beta-N-acetylglucosaminidase activity			1
microtubule minus-end binding			1
NEDD8 activating enzyme activity			1
O-methyltransferase activity			1
obsolete coenzyme binding		1	1
peptidyl-prolyl cis-trans isomerase activity		1	

peroxidase activity	1		
phosphatidylinositol binding			1
phosphatidylinositol phosphate kinase activity	1		1
phosphatidylserine decarboxylase activity		1	
polygalacturonase activity			1
potassium ion binding	1		1
protein serine/threonine kinase activity		1	
proton-transporting ATPase activity, rotational mechanism		1	
pyridoxal phosphate binding		1	1
pyruvate kinase activity	1		1
ribonuclease T2 activity			1
serine-type carboxypeptidase activity	1	1	
serine-type exopeptidase activity		1	
serine-type peptidase activity		1	
sulfate transmembrane transporter activity		1	
TBP-class protein binding		1	
threonine-type endopeptidase activity		1	
thiamine pyrophosphate binding	1		
thiolester hydrolase activity			1
transaminase activity			1
transferase activity, transferring acyl groups other than amino-acyl groups	1	2	1
translation elongation factor activity			1
transmembrane transporter activity	2	1	1
tRNA binding			1
tryptophan synthase activity		1	
unfolded protein binding			1
valine-tRNA ligase activity			1
xyloglucan:xyloglucosyl transferase activity		1	

C. Cellular Component GO Term	11-2	11-7	7-2
integral component of membrane	3	5	15
membrane	10	4	14
ribosome	1	2	8
nucleus		1	7
cytoplasm			4
chloroplast			2
chromosome			2
exocyst			2
peroxisome			2
anchored component of membrane	1		1
apoplast		1	
cell wall		1	
endoplasmic reticulum membrane	1		
extrinsic component of membrane			1
Golgi transport complex			1
nucleolus		1	
nucleosome			1
photosystem II			1
photosystem II oxygen evolving complex			1
proteasome core complex		1	
proteasome core complex, alpha-subunit complex		1	
proteasome regulatory particle, lid subcomplex	2		1
proton-transporting two-sector ATPase complex, catalytic domain		1	
transcription factor TFIIA complex	1		1

Table S9a-c. Number of CHH hypomethylated DMR-associated genes associated with each biological process (**A)**, molecular function **(B)**, and cellular component **(C)** gene ontology (GO) terms for each of the three age-contrasts (i.e. 11 – 2 year, 11 – 7 year, and 7 – 2 year). Values in each column represent the number of DMR-associated genes that are associated with each GO term. Black squares indicate no genes associated with that contrast were assigned the particular GO term.

A. Biological Process GO Term	**11-2**	**11-7**	**7-2**
protein phosphorylation	2	9	1
regulation of transcription, DNA-templated	6	9	
proteolysis	2	5	4
transmembrane transport	2	5	
carbohydrate metabolic process		3	1
obsolete oxidation-reduction process	5	3	6
translation	1	3	
ATP metabolic process		2	
base-excision repair	1	2	
nucleobase-containing compound metabolic process		2	
proton transmembrane transport		2	
response to hormone		2	
response to oxidative stress	2		2
cell redox homeostasis			1
cell wall macromolecule catabolic process		1	
chitin catabolic process		1	
defense response		1	
DNA repair		1	
DNA topological change			1
exocytosis		1	
intermembrane lipid transfer			1
intracellular protein transport	1	1	
lipid metabolic process	1		1
metal ion transport	1	1	1
nitrogen compound metabolic process			1
phytochromobilin biosynthetic process		1	
protein folding	1		
rRNA processing			1
signal transduction		1	
steroid biosynthetic process			1
sucrose metabolic process			1
superoxide metabolic process	1		
translational initiation		1	

B. Molecular Function GO Term	11-2	11-7	7-2
ATP binding	3	14	3
DNA binding	5	13	2
protein binding	4	9	3
protein kinase activity	2	9	1
zinc ion binding		6	2
cysteine-type peptidase activity	2	5	4
RNA binding		5	
sequence-specific DNA binding	4	5	
DNA-binding transcription factor activity	5	4	
metal ion binding	1	4	
ATPase activity		3	
ATPase-coupled transmembrane transporter activity		3	
protein dimerization activity	1	3	1
structural constituent of ribosome	1	3	
3'-5' exonuclease activity		2	
ADP binding	1	2	
DNA-3-methyladenine glycosylase activity	1	2	
glutathione peroxidase activity	2		2
heme binding			2
hydrolase activity	1	2	2
hydrolase activity, acting on ester bonds		2	3
iron ion binding			2
nucleic acid binding		2	4
oxidoreductase activity, acting on paired donors, with incorporation or reduction of molecular oxygen			2
polygalacturonase activity		2	
pyridoxal phosphate binding		2	
transaminase activity		2	
3-beta-hydroxy-delta5-steroid dehydrogenase activity			1
acetylglucosaminyltransferase activity	1	1	2
acid phosphatase activity		1	
carbohydrate binding		1	
catalytic activity	1	1	2
chitin binding		1	
chitinase activity		1	
cobalt ion binding		1	
DNA topoisomerase activity			1
flavin adenine dinucleotide binding	1		
hydrolase activity, hydrolyzing O-glycosyl compounds		1	1
intramolecular lyase activity		1	
lipid transfer activity			1
Lys48-specific deubiquitinase activity		1	
metal ion transmembrane transporter activity	1		1
methyltransferase activity		1	1

microtubule minus-end binding		1	
O-methyltransferase activity		1	
obsolete coenzyme binding			1
oxidoreductase activity	2		1
oxidoreductase activity, acting on the CH-OH group of donors, NAD or NADP as acceptor			1
oxidoreductase activity, acting on single donors with incorporation of molecular oxygen, incorporation of two atoms of oxygen		1	
oxidoreductase activity, acting on the CH-CH group of donors, iron-sulfur protein as acceptor		1	
polysaccharide binding	1		1
racemase activity, acting on amino acids and derivatives			1
sucrose synthase activity			1
superoxide dismutase activity	1		
thiol-dependent ubiquitin-specific protease activity		1	
transferase activity, transferring acyl groups other than amino-acyl groups		1	
transferase activity, transferring hexosyl groups	1	1	
translation initiation factor activity		1	

C. Cellular Component GO Term	11-2	11-7	7-2
integral component of membrane		5	
ribosome	1	3	
membrane	2	2	4
nucleus		2	1
cytoplasm			1
exocyst		1	

Table S10. Characterization of eight unknown proteins associated with the 17 shared DMR sequences identified among the three age-contrasts. The unknown protein ID corresponds to the unknown proteins associated with the shared DMR sequences. The putative motifs identified within each protein sequence include the position of the motif within the sequence and the e-value. The number of amino acids and estimated molecular weight (kDa) are also included for each protein sequence. Finally, the predicted localization of each protein is provided as well as the calculated probability of this prediction.

Protein ID	Putative Motifs (position and e-value)	Number of Amino Acids	Estimated Molecular Weight (kDa)	Predicted Location (probability)
unknown protein1	none found	1,122	122,388.22	chloroplast (98.98%)
unknown protein2	○ transposase_24 (213-319; $8e^{-7}$)	438	48,372.76	nucleus (50.2%)
unknown protein3	○ transposase_24 (186-312; $5e^{-11}$) ○ AbiJ N-terminal domain 4 (114-226; 0.014)	610	69,422.01	nucleus (90.87%)
unknown protein4	none found	100	11,346.45	mitochondrion (89.43%)
unknown protein5	○ DUF1336 (15-106; $5e^{-9}$) ○ DUF924 (22-89; 0.0093)	124	14,296.34	cytoplasm (93.95%)
unknown protein6	none found	339	38,963.80	nucleus (97.83%)
unknown protein7	none found	86	9,893.82	secreted pathway (85.92%)
unknown protein8	○ GIT coiled-coil Rho guanine nucleotide exchange factor (77-109; 0.0019) ○ bZIP transcription factor (76-106; 0.0033) ○ Fungal N-terminal domain of STAND proteins (54-111; 0.0084) ○ Uncharacterized protein family (UPF0242) N-terminus (54-121; 0.014) ○ Leucine-rich repeats of kinetochore protein Cenp-F/LEK1 (62-119; 0.028) ○ DUF4514 (72-146; 0.019)	158	17,972.46	nucleus (99.25%)

- Axonemal dynein light chain (47-115; 0.038)
- RNA polymerase II transcription mediator complex subunit 9 (59-117; 0.067)
- EvpB/VC_A0108, tail sheath N-terminal domain (86-141; 0.17)
- Centrosome localization domain of PPC89 (76-111; 0.3)
- Septum formation initiator (71-105; 0.47)